The G-Protein-Coupled Receptor Kinase 2 Orchestrates Hair Follicle Homeostasis

Alejandro Asensio[1,2,3], Maria Sanz-Flores[1,#], Kif Liakath-Ali[4], Julia Palacios-García[1], Jesús M Paramio[5,6,7], Ramon García-Escudero[5,6,7], Federico Mayor jr[1,2,3,8 **] and Catalina Ribas[1,2,3,8 *‡]

[1]Departamento de Biología Molecular, Instituto Universitario de Biología Molecular IUBM-UAM and Centro de Biología Molecular Severo Ochoa (UAM-CSIC), 28049 Madrid, Spain

[2]Instituto de Investigación Sanitaria La Princesa, 28006 Madrid, Spain

[3]CIBER de Enfermedades Cardiovasculares, ISCIII (CIBERCV), 28029 Madrid, Spain

[4]School of Biological Sciences, University of Southampton, Southampton, United Kingdom

[5]Molecular and Translational Oncology Division, Centro de Investigaciones Energéticas, Medioambientales y Tecnológicas (CIEMAT), Madrid, Spain

[6]Biomedical Research Institute I+12, 12 de Octubre University Hospital

[7]Centro de Investigación Biomédica en Red de Cáncer (CIBERONC)

[8]Conexión Cáncer-CSIC

[#] Present address: Cancer Research Program, Hospital del Mar Medical Research Institute, Barcelona, Spain

**Corresponding author (FM) fmayor@cbm.csic.es
*Corresponding author (CR) cribas@cbm.csic.es

[‡]Lead contact

Abstract

Tightly regulated cell-cell and cell-niche intercommunications via intertwined signaling networks are involved in maintaining normal hair follicle (HF) homeostasis, cycling and cell fate determination. However, knowledge of specific mechanisms by which hair loss takes place under pathological situations is needed. Using a keratinocyte-specific knockout mouse model, we uncover that the G-protein-coupled receptor kinase 2 (GRK2) signaling node plays a key role in HF homeostasis. Epidermal GRK2 ablation causes alterations during anagen induction, giving rise to abnormal cyst-like structures. HF-linked cysts display aberrant growth and differentiation patterns as well as lineage infidelity, displaying features of abortive HFs unable to fully acquire canonical hallmarks. Cysts triggered by GRK2 deletion displace the dermal papilla away from the bulge and promote irreversible changes in HF stem cell architecture, leading to bulge destruction and hair loss. Our data provide unforeseen roles of GRK2 in epidermal physiology and uncover mechanisms

linking dystrophic follicular cysts formation with hair loss, with potential connections to pathogenic processes operating in immune-mediated alopecias.

Keywords

Alopecia areata/Epidermal cysts/ G-Protein-Coupled Receptor Kinase 2/Hair loss/Lineage determination

Introduction

Hair follicles (HFs) constitute one of the main appendages of mammalian epidermis. They are composed of epithelial cells and have been widely used as a "mini-organ" model system for the study of adult stem cells and their differentiation processes taking place during the hair cycle [1, 2]. Hair cycle consists of three stages: growth (anagen), degeneration (catagen) and resting phase (telogen) [3]. Throughout lifetime, postnatal hair follicles undergo several cyclic rounds of destruction and regeneration, setting a system in which stem cells of resting HFs proliferate and differentiate giving rise to the hair shaft and the rest of anagen HF populations, thus making this system an ideal setting to study adult stem cell dynamics [4]. Tightly regulated spatiotemporal cell-cell and cell-niche interactions are responsible for maintaining hair homeostasis, whereas malfunctioning of any of these factors can lead to hair growth disorders such as alopecias [5].

Hair follicle stem cells (HFSC) reside in a specialized niche known as the bulge and are in charge of fueling hair growth during the first stages of the anagen phase [6, 7]. During telogen, the epithelial part of the HF includes slow-cycling bulge cells and the Hair Germ (HG) [8], a compartmentalized cluster of cells only visible during the resting phase which separates the bulge form the underlying specialized mesenchyme, the Dermal Papilla (DP) [9]. Epithelial-mesenchymal interactions are crucial during hair cycle [10-12] and the location of DP in close proximity to the HG or to the regressing HF enables a constant crosstalk between these structures, leading to the concept of DP as an orchestrator of the hair cycle, instructing the epithelial part of the HF to enter in either the regenerative or the destructive phase of the cycle [13, 14]. Several studies have pointed that bulge and HG cells not only differ in terms of their proximity to the DP, but are molecularly distinct entities, being HG cells biochemically and epigenetically primed to respond to anagen-inducing cues arising from the DP [15-17].

Cell identity within HFs is maintained by master transcription factors responsible for inducing HF commitment whilst blocking the expression of interfollicular epidermis (IFE) set of genes which are functional in other cell lineages present in the epidermis [18]. During telogen to anagen transition, complex cell signaling networks such as Shh, Notch, BMP or TGF-β [19-25] coordinately operate to induce tissue growth, regeneration and differentiation. For instance, Wnt/β-catenin pathway has a prominent role in inducing hair growth [26-29]. HFSC trigger hair production in response to Wnt signaling, and β-catenin stabilization plays a central role in the shift from TCF3/4 repressors, which are active in quiescent SCs, to Lef1, present in activated SC poised to regenerate the cycling components of the HF [30, 31]. Terminal differentiation during SC commitment takes place in a sequential manner, being the outer root sheath (ORS) and the companion layer (CL) the first to be specified, with other lineages such as matrix and inner root sheath (IRS) being generated at later stages of anagen progression [32].
A better understanding of how the different components of signaling networks crosstalk and are integrated in normal HF homeostasis, cycling and cell fate determination is needed to identify key regulatory hubs in these processes and their alterations in pathological conditions, leading to hair loss. In this regard, previous studies have reported the growth of cyst-like structures as a result of ablating signaling components relevant

for HF biology [27, 28, 33-39]. However, the mechanisms linking cyst growth with a hair loss phenotype are not well understood.

G-protein-coupled receptor kinase 2 (GRK2) was first identified as a G-protein-coupled receptor (GPCR) modulator. Its canonical role is phosphorylation of activated GPCRs, leading to the recruitment of β-arrestins, and subsequent β-arrestin-dependent receptor desensitization, internalization and signaling. In addition, GRK2 exhibits a complex cell type and context-specific repertoire of non-GPCRs partners and substrates, acting as a signaling node involved in multiple cellular processes. Through such complex interactomes, GRK2 participates in key cellular functions, whereas altered levels of this protein may play a role in the maladaptive rewiring of signaling networks taking place in different disease contexts, such as cardiovascular, tumoral or metabolic disorders [40-42].

We have previously reported that GRK2 plays a key role in preserving epithelial cell identity in the context of head and neck squamous cell carcinoma (HNSCC), which arises from the epithelium lining the oral cavity, pharynx, and larynx. GRK2 expression is reduced in undifferentiated, high-grade human HNSCC tumors, whereas its downregulation in model human HNSCC cells is sufficient to trigger mesenchymal features and enhanced malignant potential in mice models, suggesting that GRK2 is very relevant to maintain and safeguard an epithelial phenotype [43]. However, the role of this protein in HF homeostasis has not been investigated.

In this study, we utilized mouse genetics to uncover the biological role of GRK2 in this setting. We reveal that keratinocyte-specific ablation of GRK2 leads to major changes in anagen induction, hair cycling and cell lineage determination in adult mice, leading to the formation of aberrant epidermal cyst structures. Interestingly, cysts triggered by GRK2 deletion displace dermal papilla (DP) away from the bulge and promote irreversible changes in HFSC niche architecture, eventually leading to bulge destruction and hair loss. Finally, we find that cysts are destroyed during aging by mechanisms reminiscent to those described in immune-mediated alopecias. Overall, our study unravels a central role of GRK2 in hair follicle epithelial cell biology.

Results

Epidermal GRK2 deletion triggers progressive hair loss with age and early changes in hair follicle morphology along with the development of cysts upon adult hair cycling

To analyze the potential role of GRK2 in hair follicle maintenance in vivo, we specifically deleted the GRK2 gene in epidermal and hair follicle cells by crossing homozygous GRK2 floxed mice (*GRK2* $^{F/F}$) with animals harboring Cre recombinase under the Keratin14 promoter (*K14-Cre*), which directs Cre expression to Keratin14-expressing stratified epithelial compartments. Genomic characterization (Fig.S1a), immunostaining of dorsal skin sections (Fig.S1b) and western blot analysis of isolated epidermal cells (Fig.S1c) confirmed GRK2 deletion in both hair follicles (HF) and interfollicular epidermis (IFE) in the *GRK2*$^{F/F}$*;K14-Cre* mice epidermal KO animals (named GRK2 eKO from now on), whereas littermates lacking K14-Cre expression and thus retaining GRK2 floxed alleles (designated as control mice throughout the manuscript) displayed normal expression levels of GRK2.

Interestingly, we noted that although young (2 months) control and GRK2 eKO littermates were undistinguishable and displayed a normal hair phenotype, GRK2 eKO mice showed signs of hair loss with age, with an already sparser hair coat by the age of 8 months, and marked hair loss, with numerous hairless regions at 18 months (Fig.1a). Such age-related hair loss process was confirmed at the histological level (Fig.1b). Importantly, we observed that all GRK2 eKO animals exhibited abnormal epidermal cyst-like structures appearing in the dermis or linked to the lowest part of HF. These cysts were already present in 2-

142 month-old mice (Fig.1b insert), before the onset of macroscopic hair loss, and their number increased
143 significatively thereafter, peaking at 8 months (Fig.1b).
144
145 To gain insights about the dynamics of cysts growth in GRK2 eKO animals, we examined skin sections at
146 different stages of development. Importantly, GRK2 eKO pups are born without cystic structures, displaying
147 an overall normal appearance of hair follicles both in length and number compared to controls (Fig.S2a). No
148 cysts were observed either in newborns or at the first telogen stage at p21 (Fig.1c), when HF morphogenesis
149 has been completed, pointing to a specific role for GRK2 during adult HF homeostasis and cycling.
150 Consistent with this notion, all GRK2 eKO mice sections examined after second postnatal anagen (>p30)
151 showed the presence of these abnormal structures (Fig.1c). As we pointed above, dorsal skin cyst numbers
152 strongly increase by the age of 8-months in GRK2 eKO mice, when control littermates HF have usually
153 undergone circa 4 cycles, and when macroscopic hair loss effects are apparent in the knockout animals
154 (Fig.1d). Strikingly, cyst growth in adult GRK2 eKO animals was totally abrogated in ear skin, which
155 remains in a refractory telogen-arrested state for extended periods of time [44] (Fig.1d). These data suggested
156 that GRK2 may play a central role in adult HF cycling and homeostasis. To further support this notion, we
157 used a conditional mouse model of global tamoxifen-inducible GRK2 ablation (*TxCre-GRK2*$^{F/F}$). Triggering
158 GRK2 deletion at the stage of second telogen in 2-month-old mice lead with time to the same phenotype
159 observed in our constitutive epidermal specific knockout model, with major presence of cyst structures and
160 macroscopic hair loss (Fig.S2b), clearly supporting our hypothesis regarding the need of GRK2 during adult
161 hair cycling.
162
163 **GRK2 is required for proper anagen induction and progression**
164
165 We next investigated the impact of GRK2 deletion on different stages of the hair cycle. We took advantage
166 of the synchronous second telogen status (resting phase) of mouse dorsal skin HF at p55, before macroscopic
167 hair loss has started, and the possibility of triggering the synchronized anagen start via depilation.
168 During telogen, the epithelial part of the HF is composed of slow-cycling hair follicle stem cells (HFSC),
169 that reside in a specialized niche known as the bulge, the secondary Hair Germ (HG) and a specialized
170 mesenchyme, the Dermal Papilla (DP). We found that at p55 second telogen stage, both control and GRK2
171 eKO mice displayed non-significant differences in the amount of bulge HFSC, as assessed by either flow
172 cytometry (CD34$^+$ α6-integrin$^+$) or immunofluorescence (CD34$^+$, Sox9$^+$ and Keratin 15$^+$) (Fig.2a-b).
173 Interestingly however, GRK2 eKO mice exhibited smaller HG and fewer P-cadherin$^+$ HG cells per HF
174 section (Fig.2b), suggestive of an altered activation pattern of this primed HFSC compartment.
175
176 To explore the functional consequences of such alterations in the HG compartment, we depilated the p55
177 mouse back skin to induce the synchronized anagen onset and characterized HF status at 3 (D+3) or 8 (D+8)
178 days post-depilation (Fig.2c). The initial regenerative phase of hair cycle implies proliferation of HG cells,
179 eventually giving rise to the matrix by the anagen-III stage. Interestingly, proliferation of HG cells (BrdU
180 incorporation) was clearly diminished in the absence of GRK2 at D+3 post depilation (Fig.2d), indicating a
181 delay in the telogen-anagen transition. Such delay in anagen induction persisted at D+8 (Fig.2e). In control
182 animals, the high levels of proliferation were confined to the hair bulb region, sustaining the formation of
183 the hair shaft, and were indicative of canonical completion of anagen stages to a point when outer root sheath
184 (ORS) cells have ceased their expansion (Fig.2e, left)). In sharp contrast, GRK2 eKO HFs displayed a
185 retarded progression and were heterogeneous in their proliferation pattern and anagen status, ranging from
186 early anagen-III HFs with emerging matrix and proliferative upper ORS (Fig.2e, middle) to anagen-I HFs
187 where cell division can only be detected in a few HG cells (Fig.2e, right). Consistently, as judged by H&E
188 staining, in contrast to the ≥Ana-III/IV HFs observed in control littermates 8 days post depilation, with a

marked increase compared to D+3, HF length was significantly reduced in GRK2 eKO mice and remained unchanged compared to D+3 conditions (Fig.2f).

Pigmentation of mouse skin is tightly linked to the hair cycle stage and was also altered in GRK2 eKO mice. At 8 days post depilation, control and eKO skin displayed a different macroscopic appearance, with a darker grey coloration in control animals, indicative of advanced anagen stages (Fig.2g). Histological analysis and melanin staining quantification showed a significant decrease in the number of HFs displaying pigmentation in the region above the DP in GRK2 eKO mice (Fig.2g, right panels). Together, these data indicated that deletion of GRK2 in the epidermal compartment has a negative impact in anagen induction and hair cycle progression, pointing to postnatal anagen defects as one of the possible drivers of the progressive hair loss phenotype observed in GRK2 eKO mice.

HFs include a variety of cellular types with different roles throughout the cycle. To better understand the role of GRK2, we investigated the spatiotemporal dynamics of its expression in the HF. Second telogen single-cell transcriptomics (data obtained from published databases [45]) as well as our immunofluorescence staining (Fig.S3a) indicated that GRK2 is expressed in resting phase HF, with the highest signal found in the upper HF, upper bulge and HG. An additional study [16] also suggest a more dynamic expression of GRK2 transcript levels towards the late phases of telogen in HG compared to bulge cells (Fig.S3b). ATAC-Seq experiments [17] point to the same direction, with a peak of open chromatin identified in GRK2 genomic location in HG (Fig.S3c). At the protein level, we found that GRK2 levels increase over telogen bulge levels 3 days post depilation (Ana-I/II) in both bulge and HG of control HF. GRK2 levels persisted elevated in more advanced anagen stages (>Ana-III/IV), being significantly upregulated in all HF compartments and especially in the bulge, upper ORS and matrix (Fig.S3d). Altogether, it was tempting to suggest that physiological upregulation of GRK2 in HF is required for adequate anagen induction and progression, and that selective ablation in GRK2 eKO animals would trigger a delay in anagen onset and complex changes in hair cycling and HF homeostasis.

GRK2 downregulation correlates with unbalanced status of key signaling pathways involved in anagen induction and hair cycling

Given the aforementioned induction of GRK2 expression, and the fact that GRK2 has been described as a central signaling hub [40], we hypothesized that the lack of this protein may alter the activation status of signaling pathways relevant in HF homeostasis and cycling.
Robust upregulation of the LEF1 transcription factor downstream the Wnt/βCatenin pathway takes place in the HG and its progeny during telogen-anagen transition, allowing a switch from the inhibitory TCF3/4 effectors in the bulge, opposed to β-Catenin signaling [31]. Of note, consistent with the delayed anagen observed p55 GRK2 eKO mice 3 days post-depilation, these animals displayed low levels of cytoplasmic β-Catenin as well as markedly reduced nuclear Lef1 levels in the HG region compared to controls (Fig.3a). These Wnt signaling reporters remained low even at 8 days post depilation, when some eKO HFs started developing the matrix.

To analyze the long-term outcome of the mentioned altered anagen process we performed an RNASeq experiment in 8-month-old mice whole skin to detect changes in transcriptional readouts of Wnt/βCatenin and other signaling pathways. Of note, several transcripts related to HFSC were both up or downregulated in GRK2 eKO animals compared to littermates, such as Runx1, Sostdc1, Gas1, Sox9 or Fgfr2 (Fig.3b). We also detected altered levels of relevant structural proteins regarding the cytoskeleton or extracellular matrix (ECM) such as Krt79, Tnc, Itga6 or Col17a1, which are involved in HFSC aging. It is noteworthy that BMP, Wnt, GPCR and adenylate cyclase pathway signaling components and signatures were either significantly

enriched or decreased between genotypes (Fig.3c). The forementioned imbalance in signaling pathways involved in HFSC maintenance was exemplified by the significant decrease in key transcripts such as Wnt3a, Wnt7a or Acvr2b, or the increase in Tcf4 in GRK2 eKO skin (Fig.3b), overall translating into flawed "hair follicle development cytodifferentiation" signature (Fig.3c) and consistent with the alterations noted above in genes related to HFSC (Fig.3b) and to the GSEA analysis (Fig.S4). Overall, it was tempting to suggest that such alterations in cell signaling components may cooperatively act to trigger hair cycling defects and cyst emergence observed in this mouse model.

Cysts are uncoupled from normal hair follicle differentiation and cycling features

A key feature of the GRK2 eKO phenotype was the presence of abnormal cyst-like structures appearing in the dermis or linked to HF in adult mice. Since GRK2 downregulation leads to deficient anagen induction and aberrant HF cycling, we reasoned that cysts may arise in constantly cycling mouse back skin because of the accretion of such altered features over time. We thus investigated the expression of key molecular markers of HF layers in the cyst's structures (see scheme of cell layer markers found in an anagen phase hair follicle, Fig. 4a).

When skin sections were stained for HFSC markers, we observed that cysts appeared to grow from the lowest part of the HF (HG) and remained attached to the $CD34^+$ bulge, although cysts structures displayed no labeling for this HFSC marker (Fig.4b). The epidermal origin of cysts was indicated by their positive staining for Keratin 5 and high Keratin 6 labeling, whereas the lack of Keratin 15 and dim α6-integrin staining confirmed their differential features from HFSC clusters (Fig.4b and Fig.S5a). The $K6^+$ cell layer formed a continuous structure from the inner bulge stem cell niche, extending to the whole cyst (Fig.4b). Regarding anagen HF differentiation patterns, while ORS markers as K5 or P-cadherin were present in the cysts, as was the matrix ascending companion layer marker K6, the labeling of IRS determinants was markedly decreased (GATA3) or showed a non-nuclear unspecific distribution (CDP) in GRK2 eKO HF-linked cysts compared to normal HF from the same animal (Fig.4b-c). Of note, cysts showed on the inside an accumulation of eosinophilic substances that are likely keratin debris reminiscent of hair shafts and also contain lipid secretions marked by the Nile Red lipid dye (Fig.S5b), suggesting that these anomalous structures arise from HFSC clusters and remain attached to the niche yet displaying an aberrant, non-canonical differentiation program. Moreover, cyst walls appeared as a multilayered epithelium, occasionally composed by cells with enlarged and atypic nuclear morphology. (Fig.S5c). Overall, these features suggested that cysts showed features of abortive HFs unable to fully acquire the canonical anagen cell layers.
Strikingly, we observed that HF-derived cysts are not destroyed in catagen and proliferate steadily in a hair cycle stage-independent way. At p40, control HFs are synchronized in the regression phase (catagen), when no active proliferation (no Ki67) but rather destruction (caspase3) of the transient SC progeny generated during the anagen growth phase takes place (Fig.4d). However, at this catagen stage GRK2 eKO cysts cells are proliferating and contain no $Caspase3^+$ apoptotic cells, suggesting that cyst cells are unresponsive to catagen-inducing cues, thus bypassing the regression phase. Furthermore, in the p55 telogen resting phase, contrary to control HFs, active proliferation was detected in cysts (Fig.4d). Overall, these data indicated that despite being structures originated from HFs and in many cases remaining linked with them, cyst cells display an altered fate, showing growth and differentiation patterns uncoupled from normal hair cycle features.

GRK2 eKO cysts display lineage infidelity and tumoral-like features

Epidermis is comprised of two main cell lineages, the interfollicular epidermis (IFE) and HF, with differential features and cycling properties. Opposed to the cyclic and niche-induced proliferative rounds of

HF cells, interfollicular SC undergo continuous proliferation to replenish cells lost in the skin surface through desquamation. Since the proliferation patterns of cysts were reminiscent to that of IFE, we investigated the expression of key epidermal lineage determinants in our aberrant structures in 8-month-old mice. Klf5 and Sox9 are key transcription factors (TFs) demarcating IFE and HF lineages, respectively, and under homeostatic conditions its presence appears to be mutually exclusive in the same cell [18]. These TFs govern cell identity by globally controlling lineage-specific expression profiles. Strikingly, cysts showed marked staining for the IFE Klf5 TF, while remaining positive for Sox9, indicative of their HF origin. In contrast, control animals or GRK2 eKO bulges showed expression of Sox9 alone (Fig.5a and Fig.S6a). The notion of an IFE-like phenotype and lineage infidelity in cysts was further strengthened by the expression of the IFE ΔNp63 marker (Fig.5b), and an active, IFE-like proliferation pattern as assessed by BrdU incorporation (Fig.S6b). Also indicative of the altered fate of cysts, cells were positive for the infundibulum marker Lrig1, expressed only in the upper HF in control animals (Fig.5c), whereas they were negative for junctional zone markers such as Gata6 (Fig.S6c). Of note, despite displaying expression of several IFE-specific TFs and being multilayered structures, the epidermal differentiation program was not fully completed in the cysts, that lacked key markers such as K10, Filaggrin or Loricrin (Fig.S6d). This probably reflects the opposing roles and fates triggered by the HF and IFE determinants co-expressed within the cysts.

Co-expression of Klf5 and Sox9 has been described transiently during wound resolution or on a permanent basis in tumoral conditions in squamous cell carcinomas (SCCs) [18, 46]. Given that in the cysts appearing in GRK2 eKO mice, lineage infidelity takes place in “basal” conditions and is persistent over time, we searched for the presence of tumoral-related markers. Interestingly, cysts were markedly positive for the stress TF c-Jun (Fig.5d), which might contribute to the convergent expression of Sox9 and Klf5 [18]. In addition, cysts were positive for matrix remodeling or differential matrix deposition markers related to tumoral microenvironment hallmarks as TenascinC or αSMA (Fig.5d). However, despite displaying several tumoral features, GRK2 eKO mice remained skin tumor-free up to 20-month-old (Fig.S6e).

Altogether, our results put forward a crucial role of GRK2 in HF homeostasis and cycling, since its absence promotes a variety of alterations, ranging from deficient anagen induction to abnormal cell fate determination, eventually giving rise to the accumulation of aberrant HF-derived cysts uncoupled from canonical HF behavior. These data raised the questions of how cyst growth promotes progressive hair loss in GRK2 eKO mice and why cysts do not end up developing tumors despite presenting some tumoral features.

Cyst growth displaces dermal papilla (DP) away from the bulge and irreversibly affects HFSC niche architecture leading to hair loss

The mesenchymal structure located below the HFSC niche known as Dermal Papilla (DP) has been reported to be crucial in orchestrating transitions between hair cycle stages, and its proximity to the HG at the proximal part of the telogen HF enables epithelial-mesenchymal interactions [47]. During normal hair cycle, anagen HF surrounds and “pushes” the DP downwards followed by a catagen phase that returns DP to its natural place, below the bulge in telogen (Fig.6a). In sharp contrast, in GRK2 eKO mice the inability of cysts to respond to catagen-inducing signals kept the DP in contact with the cysts but away from the HFSC niche in both HF-linked cysts or in already detached structures (Fig.6b). Since the telogen HF relies in a close association between DP and HG to efficiently induce the entry into the growing phase, the fact that cysts grow out from the HG region and displaces the DP would lead cyst-bearing HF to become irreversibly telogen-arrested.

As hair cycles progress during the lifetime of the mouse, HF have the potential to add one new bulge every cycle [48], so during the first telogen HFs would be single bulged and in second telogen (p55) can display two bulges. Such unique mechanism in mouse HF, termed club hair retention, enables hair coat maintenance. Interestingly, we observed in 8-month-old GRK2 eKO mice the presence of triple-bulged HF linked to cysts, had undergone at least three hair cycles before giving rise to a cyst and the subsequent depletion of DP, indicating that these GRK2 eKO HFs had undergone at least three hair cycles before giving rise to a cyst and the subsequent depletion of their DP (Fig.S7a). Of note, cysts linked to multi-bulge HFs were always detected to be in contact with the newest bulge (Fig.S7b), consistent with the notion of irreversible telogen arrest and hair growth impairment following cyst-induced DP displacement in GRK2 eKO animals.

We next explored the long-term consequences in bulge homeostasis and architecture triggered by aberrant cyst growth. Organization of HFSC within the niche is crucial to maintain SC function and genes related to ECM and bulge structure have been suggested to be critical during aging [49]. Control bulges display the typical bulge architecture comprised of two cell layers, the outer one essential during the regeneration process and the inner layer acting mainly as an anchoring point of the club hair to the HF and promoting quiescence through anagen inhibitory signals [4]. In contrast, histological examination of 8-month-old GRK2 eKO HFs giving rise to cysts showed a disorganized pattern, where the two bulge cell layers were not well distinguished and a pale and more eosinophilic labeling points to an altered differentiation state (Fig.6c). Co-immunofluorescence staining confirmed that cyst-linked HFs show structural alterations in the bulge region correlating with the loss of canonical HFSC markers. In control HF bulges, the outer cell layer was enriched in both P- and E-cadherins, whereas inner bulge cells only expressed E-cadherin. In contrast, cyst-linked GRK2 eKO HFs displayed a continuous and delocalized staining for both cadherins, coherent with the observed miss- organization of the outer and inner bulge cell layers that seem to be interspersed together. Consequently, adherens junctions, which rely on cadherin-cadherin homophilic interactions, were aberrantly distributed in GRK2 eKO compared to controls, as judged by ZO-1 and β-Catenin staining. Moreover, the inner bulge enrichment in F-actin staining detected in control animals was lost in GRK2 eKO littermates, indicating that alterations also extended to the cytoskeletal architecture and reflecting that structural miss-organization affects the whole bulge. Accordingly, bulges affected by these architectural changes triggered by cyst outgrowth in GRK2 eKO mice had lost most of CD34 expression compared to controls (Fig.6c). The analysis of aged (18-month-old) mouse skin sections further indicated that HFs linked to cysts were not only CD34 negative, but had progressed further in the degeneration process, displaying no obvious bulge structure in the lower region of the HF (Fig.6d), thereby triggering a striking decline in GRK2 eKO bulge numbers throughout aging as hair cycles take place (Fig.6e).

Consistent with the overall notion of delayed HF cycling, cyst formation in a fraction of HFs, altered niche architecture and hair loss in GRK2 eKO mice, the analysis of GRK2 knockout mice until day 20 post-depilation at p55 revealed that anagen induction resulted in a notable increase in cyst numbers when compared to that of 2nd telogen phase (Fig.S7c). In this line, we noted that repetitive depilation, that would trigger several rounds of hair growth, exacerbates the GRK2 eKO phenotype. GRK2 eKO mice did grow a sparser hair coat than control animals when subjected to repetitive depilation. In contrast to control littermates, hair coat recovery was already severely compromised after 6 rounds of depilation in GRK2 eKO (Fig.S7d), and these depilated mice showed marked hair loss and a patent decrease in both HFSC CD34^{+} bulge cells and in total bulge structures by the end of the experiment after 9 depilation rounds (Fig.S7e). These data indicated that repetitive depilation aggravates stem cell exhaustion in GRK2 eKO mice correlating with the inability to regrow hair, and mechanistically argues in favor of the proposed model of HFSC niche architecture alterations and bulge destruction as a driver of hair loss in these animals.

Overall, our data indicate that cysts have long-term consequences on the HFSC niche architecture in GRK2 eKO mice, eventually leading to loss of bulge homeostasis and hair loss. According to our hypothesis, the

379 more hair cycles that occur as mice age, the more HFs would be converted to cysts, thereby compromising
380 DP-bulge interactions and bulge functionality, leading to the phenotype observed in GRK2 eKO mice.
381
382
383 **Epidermal cysts are destroyed during aging by mechanisms resembling immune-mediated alopecia**
384
385 Our data thus far pointed to a very relevant role of GRK2 in HF homeostasis, since its absence leads to
386 deficient anagen induction, abnormal cell fate determination, and accumulation of aberrant HF-derived cysts
387 uncoupled from canonical HF behavior, eventually promoting structural changes in the HFSC niche, bulge
388 destruction and hair loss.
389
390 Intriguingly, the persistence of lineage infidelity in basal conditions within cysts was reminiscent of that
391 observed during wound healing or epithelial tumorigenesis [18]. However, cysts did not end up developing
392 tumors throughout aging in GRK2 eKO mice, despite the presence of several tumoral markers, suggesting
393 the existence of compensatory or counteracting processes. In fact, we observed that the number of cysts in
394 GRK2 eKO animals reached a peak at 8 months of age and declined in 18-month-old mice, suggesting that
395 HF-derived cysts are destroyed during aging (Fig.7).
396 In the context of epithelial cell tumorigenesis, immune-epithelial interactions are of key importance [50]. In
397 control mice, the presence of immune cells was restricted to the infundibular region, whilst the bulge displays
398 what is termed the immune privilege [51]. However, in mutant animals CD45-positive immune cells were
399 not only located in such area, but largely present in the vicinity of HFs and cysts, either inside cysts or
400 surrounding them (Fig.7a-b).
401 Detailed observation of the cysts led us to classify them into three groups according to their morphology,
402 structural integrity, and degree of immune infiltration: i) healthy-looking cysts with a rounded morphology
403 and CD45 cells nearby; ii) cysts that started losing their characteristic morphology and displayed infiltration
404 of immune cells; and iii) remnants of destroyed cyst free in the dermis (Fig.7b). We also observed that the
405 proportion of cysts showing structural integrity markedly decreases with age, with a concomitant increase
406 in the number of compromised or destroyed cysts, in which a prominent loss of epidermal markers such as
407 E-cadherin is noted (red arrowheads) compared to rounded, "healthy" cysts (blue arrowheads) (Fig.7c).
408 These observations were consistent with the aforementioned decrease in the total numbers of cysts in aged
409 (18-month-old) mice (Fig.7c).
410 Of note, we observed that cells in cysts displayed abnormal nuclear morphology with characteristic DNA
411 condensation patterns as well as positive staining for γ-H2AX (Fig.7d), indicative of DNA damage. In aged
412 mice, where HFs are no longer synchronized, we detected cysts with irregular morphology showing positive
413 staining for apoptotic markers (cleaved caspase 3 and TUNEL) (Fig.7d), indicative of the destruction and
414 clearance of cysts from the GRK2 eKO aging skin via apoptosis at these latter stages.
415
416 Regarding $CD45^+$ immune infiltrates, among the immune cell subpopulations present in cysts, we noticed a
417 prominent presence of $CD3^+$ T cells located both in the dermis surrounding cysts and within the epidermal
418 cyst cell layers (Fig.7e), many of which were confirmed to be $CD4^+$ T cells. Increased expression of adhesion
419 molecules (ICAM1) in cysts might be mediating such immune cell recruitment. As reported in situations of
420 HF immune privilege collapse [52], MHC-II-expressing immune cells are present in the vicinity of cysts,
421 along with the presence of $F4/80^+$ macrophages within destroyed cysts, surrounding cells, and wrapping
422 their membrane around cell nuclei with irregular morphology (Fig.7e).
423
424 Collapse of the immune privilege and immune cell infiltration is one of the key features of the development
425 of immune-mediated alopecias such as alopecia areata (AA) [53]. Strikingly, the phenotype of GRK2 eKO
426 mice shared other several central hallmarks of AA. 18-month-old GRK2 eKO mice hair coat exhibited the

presence of exclamation mark hairs (Fig.S8a), the prime diagnostic feature of AA [54], together with Keratin debris consistent with hair shaft fragility (Fig.S8b), or the presence of severe dermal inflammation involving polymorphonuclear cells such as neutrophils, macrophages and even foreign-body giant cells (black arrowhead, Fig.S8c). AA is also associated with leading melanin deposition in the dermis owing to the destruction of the follicular epithelium, termed as pigmentary incontinence [55]. Using electron microscopy and histochemical approaches we detected the presence of melanin in cysts at any stage, either inside healthy structures as well as free in the dermis or in the remnants of cysts that had already undergone immune-mediated destruction (Fig.S8d). Moreover, the skin of 8-month-old GRK2 eKO animals shared transcriptomic features of AA. The genes overexpressed in the skin of GRK2 eKO mice (GRK2 eKO signature) are significantly enriched in the affected skin with alopecia from the C3H mouse model, as well as in affected skin samples from AA patients (Fig.7f). Similarly, the genes overexpressed in affected skin samples from AA patients (human AA signature) are significantly enriched in the skin of GRK2 eKO mice (Fig.7g). Even when the GRK2 eKO phenotype shares several transcriptomic and histopathological similarities with AA, analysis of *GRK2* transcript levels in whole skin samples obtained from different types of AA patients (GSE68801) [56] did not correlate with disease (Fig.S8e). This could be due to the "dilution" of local GRK2 expression changes in whole skin samples, given its ubiquitous expression in different cell types, or reflect transient changes in different stages of disease progression.

Overall, our data indicated that GRK2 is essential for HF homeostasis, its deletion leading to complex alterations in HF cycling features and cell fate determination, eventually leading to the development of epidermal cysts that are destroyed during aging by mechanisms reminiscent of those operating in immune-mediated alopecias.

Fig.1

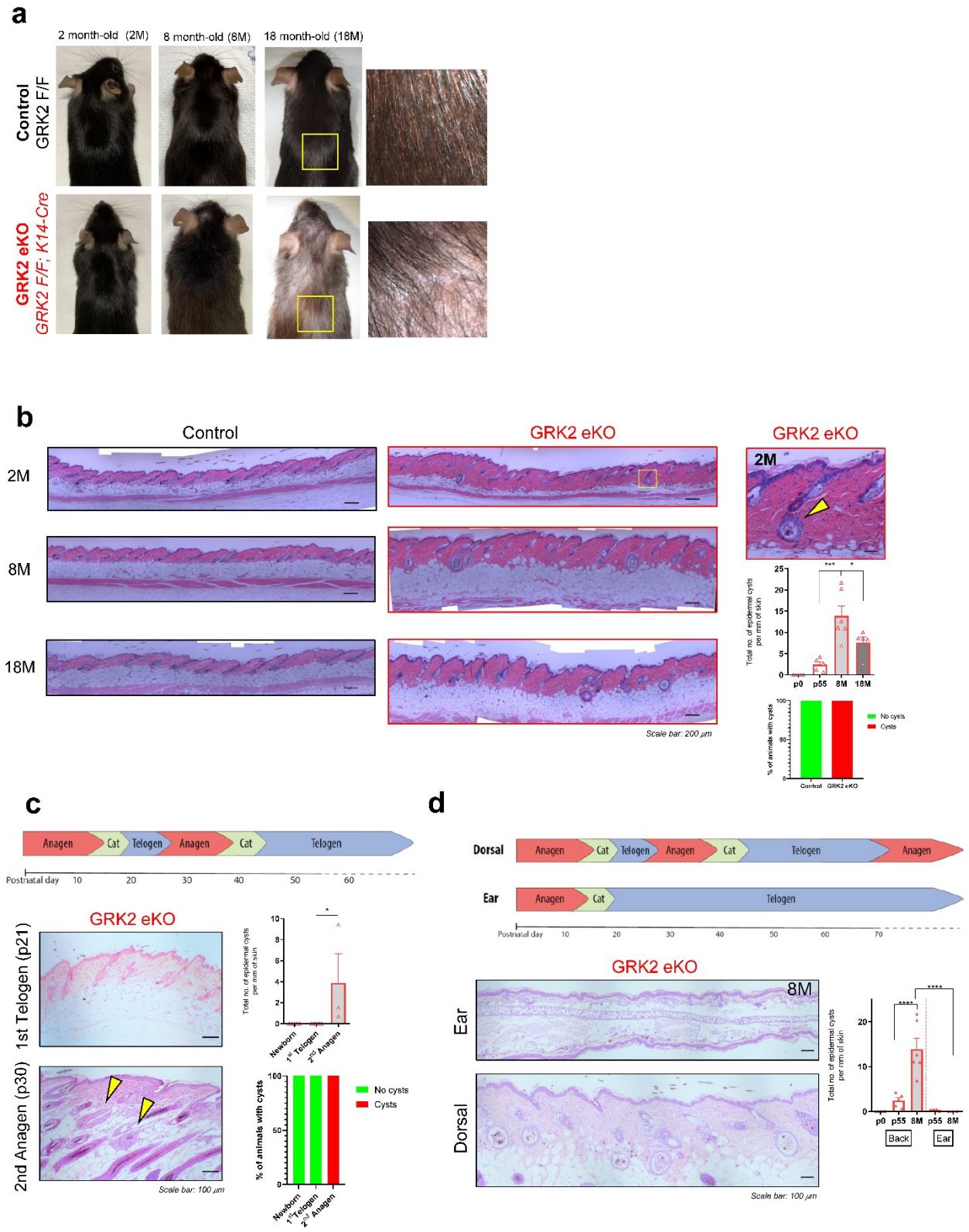
a
2 month-old (2M)
8 month-old (8M)
18 month-old (18M)
Control
GRK2 F/F
GRK2 eKO
GRK2 F/F; K14-Cre
b
Control
GRK2 eKO
GRK2 eKO
2M
8M
18M
2M
Scale bar: 200 μm
Total no. of epidermal cysts per mm of skin
p0
p55
8M
18M
% of animals with cysts
No cysts
Cysts
Control
GRK2 eKO
c
Anagen
Cat
Telogen
Anagen
Cat
Telogen
Postnatal day
10
20
30
40
50
60
GRK2 eKO
1st Telogen (p21)
2nd Anagen (p30)
Scale bar: 100 μm
Total no. of epidermal cysts per mm of skin
% of animals with cysts
No cysts
Cysts
Newborn
1st Telogen
2nd Anagen
d
Dorsal
Anagen
Cat
Telogen
Anagen
Cat
Telogen
Anagen
Ear
Anagen
Cat
Telogen
Postnatal day
10
20
30
40
50
60
70
GRK2 eKO
8M
Ear
Dorsal
Scale bar: 100 μm
Total no. of epidermal cysts per mm of skin
p0
p55
8M
p55
8M
Back
Ear

450

Fig.2

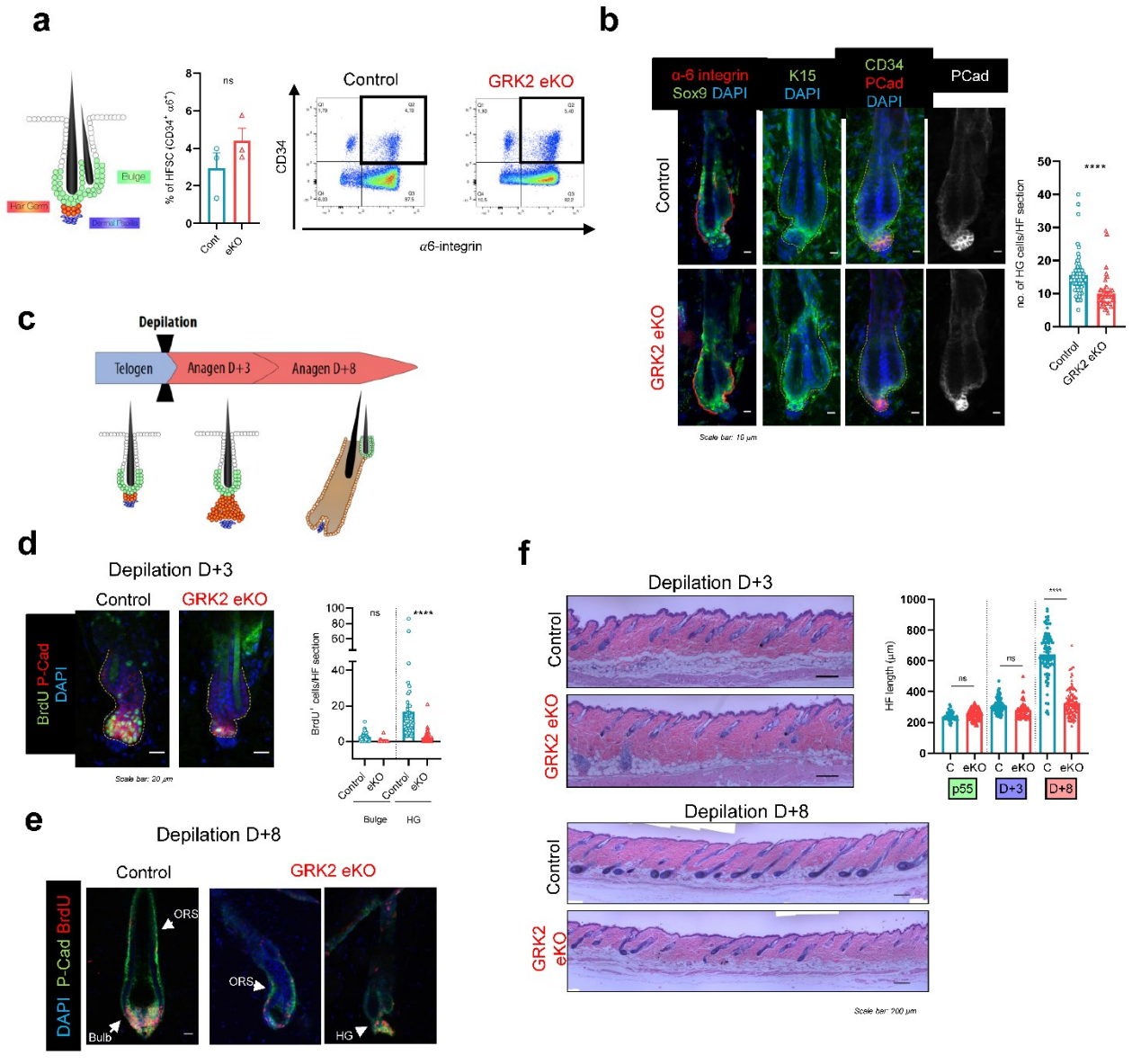
a
Bulge
Hair Germ
Dermal Papilla
% of HFSC (CD34+ α6+)
ns
Cont
eKO
Control
GRK2 eKO
CD34
α6-integrin
b
α-6 integrin
Sox9 DAPI
K15
DAPI
CD34
PCad
DAPI
PCad
Control
GRK2 eKO
no. of HG cells/HF section
****
Control
GRK2 eKO
Scale bar: 15 μm
c
Depilation
Telogen
Anagen D+3
Anagen D+8
d
Depilation D+3
Control
GRK2 eKO
BrdU P-Cad
DAPI
Scale bar: 20 μm
BrdU+ cells/HF section
ns
****
Control
eKO
Control
eKO
Bulge
HG
e
Depilation D+8
Control
GRK2 eKO
DAPI P-Cad BrdU
ORS
ORS
Bulb
HG
f
Depilation D+3
Control
GRK2 eKO
HF length (μm)
ns
ns
****
C
eKO
C
eKO
C
eKO
p55
D+3
D+8
Depilation D+8
Control
GRK2 eKO
Scale bar: 200 μm
g
GRK2 eKO
Control
BF
Fontana-Masson
melanin staining
Control
GRK2 eKO
Scale bar: 100 μm
Scale bar: 100 μm
HF showing pigmentation/mm
(≥ Ana III)
**
Cont
eKO

451

Fig.3

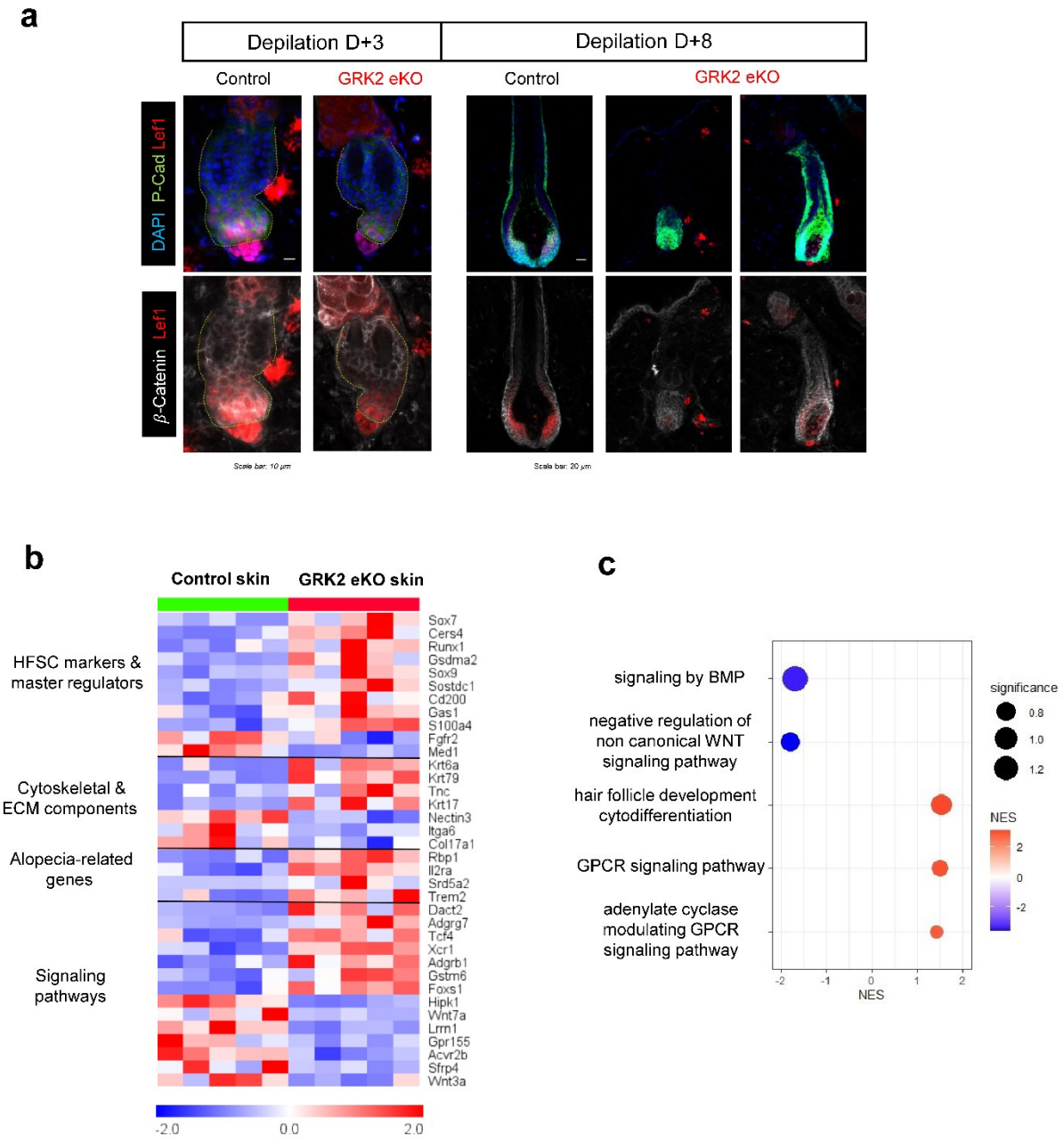
a
Depilation D+3
Depilation D+8
Control
GRK2 eKO
Control
GRK2 eKO
DAPI P-Cad Lef1
β-Catenin Lef1
Scale bar: 10 μm
Scale bar: 20 μm
b
Control skin
GRK2 eKO skin
HFSC markers & master regulators
Cytoskeletal & ECM components
Alopecia-related genes
Signaling pathways
Sox7
Cers4
Runx1
Gsdma2
Sox9
Sostdc1
Cd200
Gas1
S100a4
Fgfr2
Med1
Krt6a
Krt79
Tnc
Krt17
Nectin3
Itga6
Col17a1
Rbp1
Il2ra
Srd5a2
Trem2
Dact2
Adgrg7
Tcf4
Xcr1
Adgrb1
Gstm6
Foxs1
Hipk1
Wnt7a
Lrrn1
Gpr155
Acvr2b
Sfrp4
Wnt3a
-2.0
0.0
2.0
c
signaling by BMP
negative regulation of non canonical WNT signaling pathway
hair follicle development cytodifferentiation
GPCR signaling pathway
adenylate cyclase modulating GPCR signaling pathway
-2
-1
0
1
2
NES
significance
0.8
1.0
1.2
NES
2
0
-2

452

Fig.4

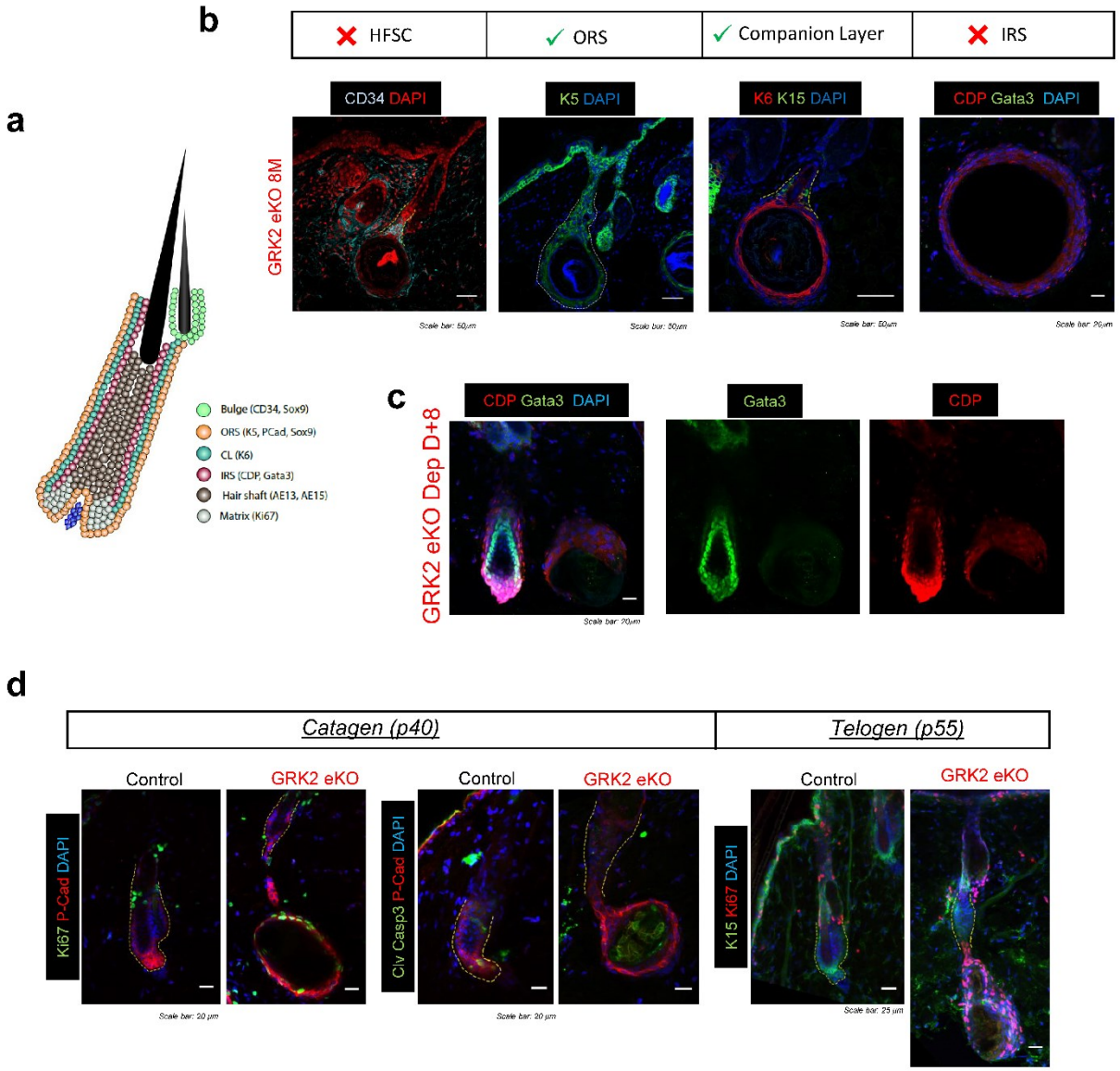
a
b
HFSC
ORS
Companion Layer
IRS
CD34 DAPI
K5 DAPI
K6 K15 DAPI
CDP Gata3 DAPI
GRK2 eKO 8M
Bulge (CD34, Sox9)
ORS (K5, PCad, Sox9)
CL (K6)
IRS (CDP, Gata3)
Hair shaft (AE13, AE15)
Matrix (Ki67)
c
CDP Gata3 DAPI
Gata3
CDP
GRK2 eKO Dep D+8
d
Catagen (p40)
Telogen (p55)
Control
GRK2 eKO
Ki67 P-Cad DAPI
Clv Casp3 P-Cad DAPI
K15 Ki67 DAPI

453

Fig.5

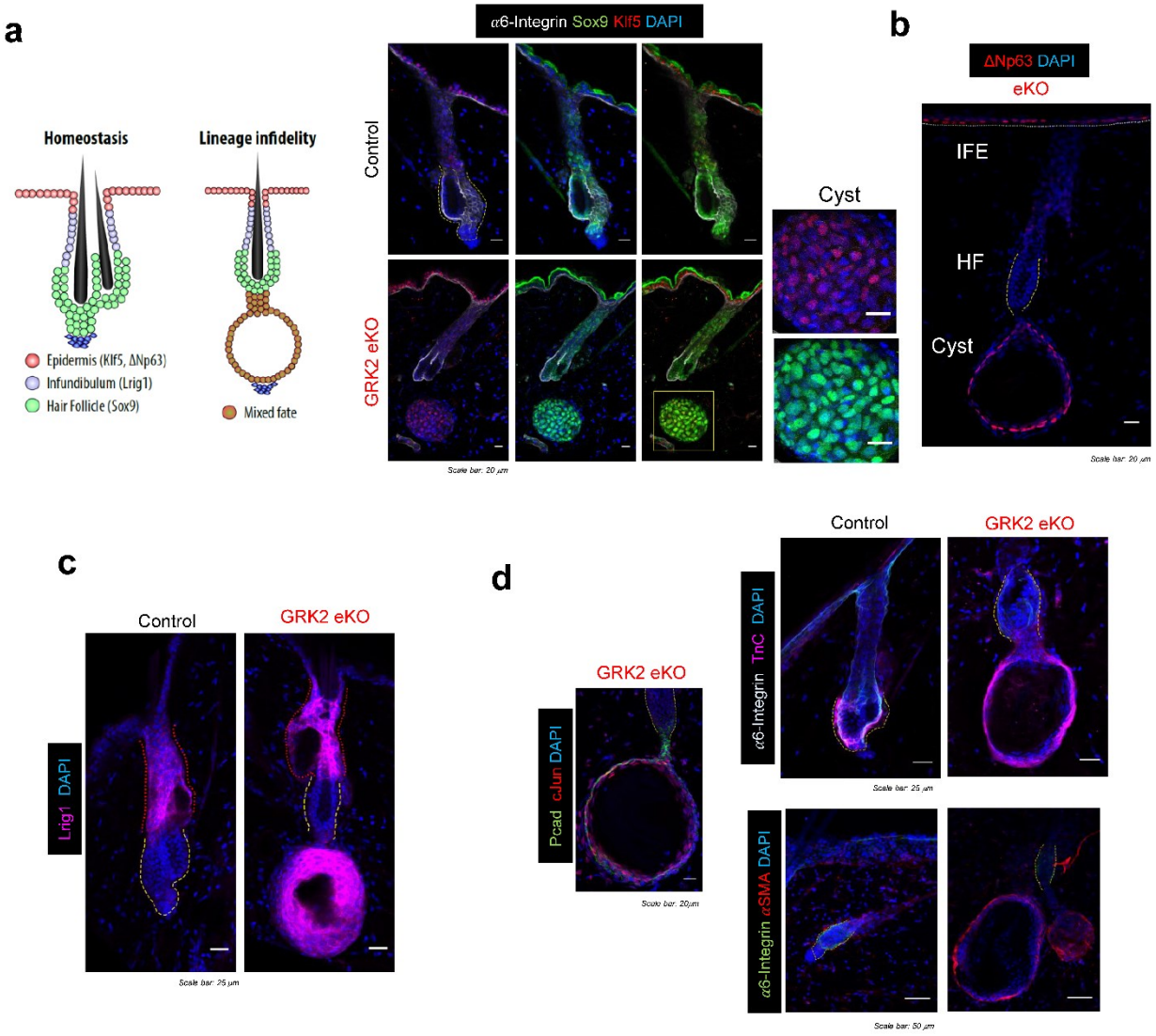
a
Homeostasis
Lineage infidelity
Epidermis (Klf5, ΔNp63)
Infundibulum (Lrig1)
Hair Follicle (Sox9)
Mixed fate
α6-Integrin Sox9 Klf5 DAPI
Control
GRK2 eKO
Cyst
Scale bar: 20 μm
b
ΔNp63 DAPI
eKO
IFE
HF
Cyst
Scale bar: 20 μm
c
Control
GRK2 eKO
Lrig1 DAPI
Scale bar: 25 μm
d
GRK2 eKO
Pcad cJun DAPI
Scale bar: 20μm
Control
GRK2 eKO
α6-Integrin TnC DAPI
Scale bar: 25 μm
α6-Integrin αSMA DAPI
Scale bar: 50 μm

454

Fig.6

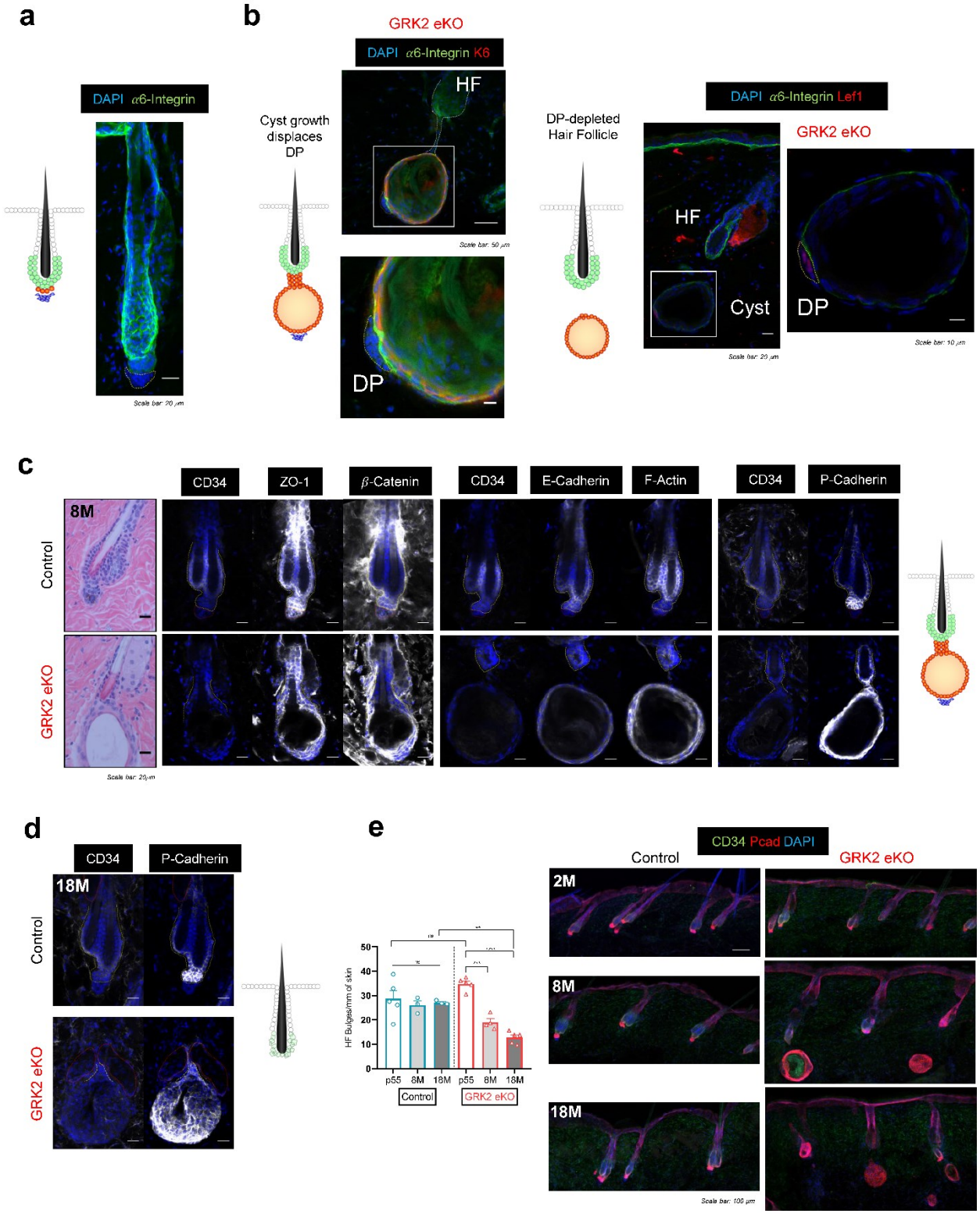
a
DAPI α6-Integrin
Scale bar: 20 μm
b
GRK2 eKO
DAPI α6-Integrin K6
HF
Cyst growth displaces DP
Scale bar: 50 μm
DP
DP-depleted Hair Follicle
DAPI α6-Integrin Lef1
GRK2 eKO
HF
Cyst
Scale bar: 20 μm
DP
Scale bar: 10 μm
c
CD34
ZO-1
β-Catenin
CD34
E-Cadherin
F-Actin
CD34
P-Cadherin
8M
Control
GRK2 eKO
Scale bar: 20 μm
d
CD34
P-Cadherin
18M
Control
GRK2 eKO
e
HF Bulges/mm of skin
50
40
30
20
10
0
p55
8M
18M
p55
8M
18M
Control
GRK2 eKO
CD34 Pcad DAPI
Control
GRK2 eKO
2M
8M
18M
Scale bar: 100 μm

455

Fig.7

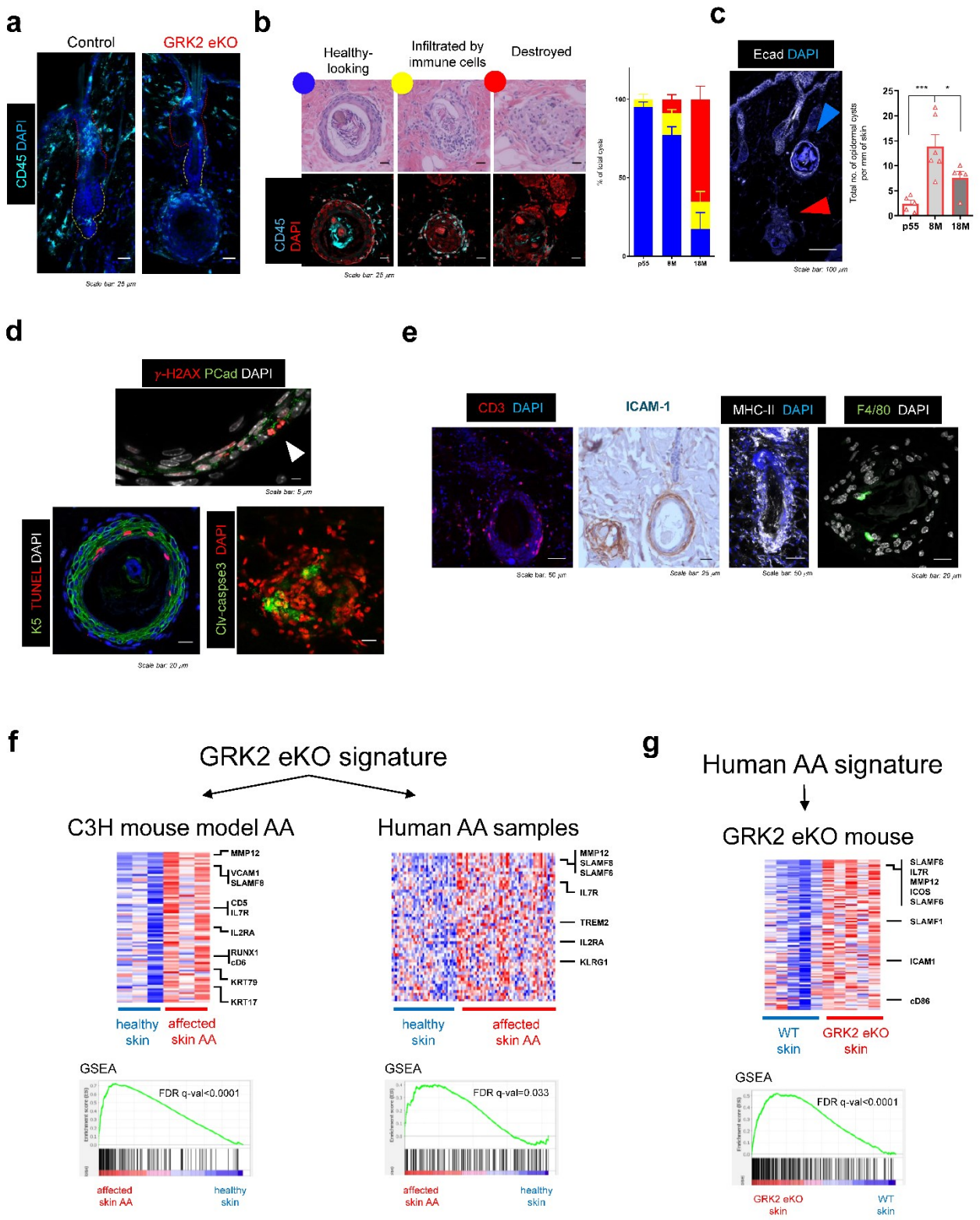

456
457
458
459
460

Discussion

Tightly regulated spatiotemporal cell-cell and cell-niche intercommunications, as those involving Bulge-HG-DP crosstalk, take place via multiple stimuli and signaling cues that act through cell signaling networks and are responsible for maintaining normal HF homeostasis, cycling and cell fate determination [15, 17, 21, 22]. Using a keratinocyte-specific knockout mouse model, we uncover that GRK2 as a signaling node plays a central role in hair follicle biology.

A specific role for GRK2 during adult HF homeostasis and cycling is indicated by the facts that: i) the phenotype observed in GRK2 eKO mice is independent of HF morphogenesis; ii) cyst growth is only observed in cycling regions of adult GRK2 eKO animals, being absent in refractory and telogen-arrested regions as the ear skin [44]; iii) triggering global tamoxifen-inducible GRK2 ablation at the stage of second telogen in 2-month-old mice mimics the constitutive epidermal KO model.

Early alterations in GRK2 eKO HFs involve decreased hair germ size and unusual hair cycling features. Slow-cycling HFSC building up the bulge during telogen sharply differ from their activated counterparts residing in the HG [47]. GRK2 deletion selectively leads to HG shrinkage during the second telogen, leaving bulge HFSCs unaffected. Moreover, depilation experiments in p55 back skin indicated a delay in the telogen-anagen transition in GRK2 eKO animals, along with a retarded and heterogeneous progression in their proliferation pattern and anagen status, reduced HF length and pigmentation, all indicative of altered hair cycle progression, and consistent with the need of a fully functional HG to correctly achieve tissue regeneration.

HGs can be derived from catagen-surviving cells [4, 57] or from bulge cells migrating downwards during the catagen-telogen transition to acquire a HG fate [8, 58]. Although we observe equal or even slightly higher numbers of HFSC in GRK2 eKO mice at p55 compared to control, the possibility of a defective migration of quiescent SC to replenish HG cannot be ruled out. Since a smaller HG has been related with a delay in anagen entry [21], it may also be feasible that since we find that anagen entry takes place at later timepoints as a consequence of GRK2 deletion, HG formation during catagen-telogen transition might as well be delayed in GRK2 eKO mice.

Although both bulge and HG contribute to hair cycling during anagen, a smaller HG has been related with a delay in anagen entry [21]. The upper HG gives rise to ORS cells during anagen [59, 60], whereas the proximal part in close contact with the DP proliferates first by the end of the telogen phase and generates the matrix [15]. Matrix development is more severely altered than that of ORS in GRK2 eKO mice, suggesting that the region of the HG in closer contact with the DP would be more affected by the lack of GRK2. However, HFs with laser-ablated HG can recover normally with a minor SC input during anagen [14], suggesting that HG abnormalities alone will not account for our whole anagen delay phenotype, and that HFSC dysfunction due to the absence of GRK2 would play a role as well. Since HG may also contribute to keep the quiescent pool of stem cells in the bulge away from the DP-derived proliferative signals [47], a smaller HG may hamper such “isolation” and favor HFSC exhaustion and premature aging in the long-term [21], as observed in GRK2 eKO mice. Consistent with a central role for GRK2 within the stem cell niche compartment and during adult hair cycling, we have uncovered a dynamic modulation of GRK2 levels during the different hair cycle stages. A higher and more dynamic regulation of GRK2 transcript levels is noted towards the final phases of telogen in HG compared to bulge cells, and GRK2 protein levels are higher at 3 days post depilation in both HG and Bulge cells and remain high up to 8 days post depilation in advanced anagen IV-VI stages, suggesting that HG and anagen HFs are poised to upregulate GRK2 during telogen to anagen transition, while keeping GRK2 under a certain critical threshold would alter HG homeostasis, and

506 thereby hair regeneration, as observed in GRK2 eKO mice. The signals and mechanisms underlying such
507 dynamic changes in GRK2 expression remain to be investigated.

508 We postulate that the altered hair cycling features of GRK2 eKO animals give rise over time to the abnormal
509 cyst-like structures, specifically emerging only in hair-cycling areas both by standard hair cycling as well as
510 by depilation-induced hair regeneration. Despite originating from the lowest part of the HF (HG) and often
511 remaining attached to the bulge (although not displaying HFSC labeling) GRK2 eKO cysts display aberrant
512 growth and differentiation patterns. Cysts proliferate steadily in a hair cycle stage-independent way, are not
513 destroyed in catagen, and display features of abortive HFs unable to fully acquire all the canonical anagen
514 cell layers. Cysts can acquire ORS fate, one of the first structures produced during hair growth [3] and
515 display as well markers of the matrix ascending companion layer, but the generation of IRS is compromised,
516 probably linked to the absence of Gata3 expression, crucial for matrix cells to be transformed into the IRS
517 layer [61]. Such defective IRS commitment may derive from an impairment in the generation of IRS
518 progenitor structures or reflect a direct involvement of GRK2 in IRS maturation, both deriving into the
519 formation of dystrophic hair follicles or cysts. Other authors [28, 37, 62-65] have reported contexts in which
520 IRS is not correctly formed, typically within a phenotype affecting adult HFs but not hair morphogenesis.
521 Why aberrant IRS formation debuts in the first's postnatal hair cycles despite IRS fate is specified in a similar
522 manner in both adult and morphogenesis stages [32] remains to be determined.

523 Our data also imply that although GRK2 ablation would lead to a general delay in hair cycle, as noted upon
524 forced anagen induction through depilation, only a fraction of HFs would transform into cysts, whereas other
525 follicles would undergo several rounds of hair cycles before developing cysts. Observing triple-bulged HF
526 linked to cysts further strengthen this idea. Once the cysts start to develop, they proliferate steadily in a hair
527 cycle stage-independent way, do not regress during catagen, and display an altered fate and lineage infidelity.

528 Strikingly, in GRK2 eKO mice, the DP rather than being engulfed by the HF remains located in contact with
529 the proximal part of the dysplastic HF, being pushed away and displaced from the HG as cysts grow during
530 anagen, thus promoting changes in HF stem cell architecture, linking cysts with hair loss. Our observations
531 regarding cyst location always being beneath the newest bulge reinforces the idea of cyst emergence being
532 associated with telogen arrest. However, contrary to what has been described in Hairless mice, GRK2 eKO
533 animals show an evenly distributed proliferation status along cycle stages and cysts regions, in contrast to
534 the proximal localization expected if this process was only dependent on paracrine DP stimuli. Therefore, it
535 is tempting to suggest that the lack of cyst growth coordination with DP signals is determined by the lack of
536 adequate responsiveness to DP-derived cues, rather than due to DP miss-localization as described [14, 66].
537 Overall, our data point to a self-generated growth potential within these epidermal cysts, independent from
538 the growth-inducing cues emanating from the DP compartment.

539 In this regard, the fact that epidermal cysts arising in GRK2 eKO conditions display a multilayered
540 epithelium expressing IFE-like differentiation and ORS/CL markers, but not IRS or late epidermal
541 differentiation features, pointed to the occurrence of altered cell lineage determination processes. Klf5 and
542 Sox9 have been described as master transcription factors (TF) demarcating IFE and HF lineages,
543 respectively, and under homeostatic conditions its presence is mutually exclusive [18]. Strikingly, we find
544 that both uni-lineage determinants are co-expressed inside cysts, a process known as lineage infidelity. The
545 expression of Klf5 in cysts together with ΔNp63, which expression is typically restricted to IFE, may provide
546 a causative explanation for their unresponsiveness to hair cycle-associated signals. Importantly, cyst cells
547 not only display a shifted TF landscape, but also show a remodeled environment with the presence of
548 tumoral-associated markers, and the stress TF c-Jun, which might contribute to the convergent expression
549 of Sox9 and Klf5 [18].

It is tempting to suggest that cysts outgrowth in GRK2 eKO animals might phenocopy tumoral initiation stages, where lineage infidelity is known to provide cancer cell clusters with a heterogeneous and more plastic phenotype enabling tumor survival [46]. Bulge-targeted oncogene activation has been reported to drive tumoral growth specifically during anagen phase, when the environment is permissive with HFSC proliferation, concomitant with the emergence of cyst-like structures with marked similarities to our GRK2 eKO model [39]. The capacity of HF cells to give rise to tumors with mesenchymal features and higher malignant potential has been described [67]. In a previous study [43], we found that GRK2 loss in head and neck cancer cells triggers cell fate switching from epithelial to more mesenchymal features leading to tumor progression. Nevertheless, despite showing certain tumoral hallmarks, GRK2 eKO cysts do not further progress into SCC, at least in basal conditions, despite persistent lineage infidelity.

Our results put forward GRK2 as an integrative hub in signaling pathways related to HF homeostasis, in line with its reported participation in the modulation and crosstalk of multiple signaling networks in a cell type and context-dependent way [40, 42]. We suggest that GRK2 downregulation would simultaneously and cooperatively affect highly interconnected signaling cascades relevant to HF homeostasis and cycling, including decreased activation status of the Wnt/β-Catenin/Lef1 pathway, or unbalanced expression of transcripts related to networks involved in HFSC maintenance such as Wnt, BMP, or GPCR/adenylate cyclase/PKA pathways (see scheme in Fig.S9).

In this regard, truncated Lef1 expression in skin keratinocytes (ΔNLef1), which abolishes Wnt/βCat signaling [28], causes a mouse phenotype reminiscent to that of GRK2 eKO mice, with a delayed anagen, cyst growth and absence of IRS markers, consistent with the presence of Lef1 regulatory elements in hair-specific keratins promoters [68, 69]. Interestingly, GRK2 loss-of-function mutations in Jeune syndrome patients can lead to a defective response to Wnt ligands in chondrocytes due to the impaired phosphorylation of the Wnt co-receptor Lrp6 [70]. A BMP receptor KO mouse model (Bmpr1a KO) can correctly form the ORS but not the IRS layer during anagen, deriving in a multilayered epithelium full of keratin debris [34], with clear parallelisms with our mice phenotype. Spatiotemporally controlled Smad 2/3 and Smad 1/5/8 signals are required to achieve correct follicular homeostasis downstream TGFβ and BMP receptors, being the Smad2 cascade relevant during anagen induction [24] and the BMP signal required to form IRS [32]. Since GRK2 can modulate TGFβ signaling via its ability to phosphorylate Smad2 [71], and GRK2 downmodulation unbalances endothelial TFGβ networks [72], it is tempting to suggest that unbalanced Smads activation upon GRK2 loss may contribute to the observed hair follicle phenotype. Of note, labeling of ΔNp63, a signaling node related to Wnt and other pathways is detected in GRK2 eKO cysts, and overexpression of this factor prevents follicular cells to give rise to IRS and matrix cell populations and their shift in terms of epidermal and HF master regulators [73, 74]. On the other hand, GRK2 has been recently reported to exert a positive role in Hedgehog (Hh) signaling by relocating towards the ciliary base upon Smo GPCR-like receptor stimulation, allowing Smo phosphorylation and its subsequent interaction with the PKA-C catalytic subunit [75, 76], which eventually would relieve the inhibitory phosphorylation of GLI2, allowing the activation of downstream genes. Thus, GRK2 silencing would favor enhanced activation of the PKA cascade, consistent with the observed upregulation of GPCR/adenylate cyclase pathways signatures in our RNAseq data. It is worth noting that conditional epidermal deletion of Gαs (Gnas), a major regulator of the GPCR/Adenylyl cyclase/cAMP/PKA pathway, is alone sufficient to cause aberrant expansion of the stem cell compartment and rapid formation of basal cell carcinoma (BCC) in the skin, in a way dependent on decreased PKA activation status in such conditions, leading to activation of Hedgehog GLI and Hippo YAP1 transcriptional networks. On the contrary, persistent expression of the constitutive mutant active form GαsR201C in basal keratinocytes led with time to HF stem cell depletion and progressive hair loss via reduction of GLI and YAP1 transcriptional activity, with HFs terminally differentiating into keratinized cyst structures [77]. Thus, constitutively enhancing the adenylyl cyclase/cAMP/PKA pathway would favor the inhibitory phosphorylation by PKA towards the Hh cascade. Of note, the phenotype observed upon active

597 Gαs expression shares common features with our GRK2 eKO model. Altogether, we propose that GRK2
598 downregulation could simultaneously affect the highly interconnected Wnt, BMP and Hh signalling
599 pathways, thus impairing HF homeostasis.
600 Overall, the fact that several targeted genetic modifications involving crucial HFSC signaling components
601 disturb hair follicles phenotype in ways closely resembling that triggered by GRK2 depletion, stresses the
602 importance of GRK2 as a regulatory node in HF homeostasis and lineage specification during adult hair
603 cycle.

604 Hair loss observed in GRK2 eKO animals starts much sooner than age-related hair loss [78], and appears to
605 be linked to the progressive emergence of HF-derived cysts. Regarding the mechanisms involved, we
606 uncover that GRK2 ablation in keratinocytes promotes key alterations in the HF stem cell niche.
607 Mesenchymal-epithelial crosstalk enabled by the proximity between DP and HF is required for supporting
608 epithelial cell growth throughout hair cycle [9, 12, 16, 79] and to maintain the molecular signature and hair-
609 inductive properties at the stem cell niche [80]. In GRK2 eKO mice, the inability of cysts to respond to
610 catagen-inducing signals leaves the DP in contact with the cysts but away from the HFSC niche, thus
611 disturbing such homeostatic crosstalk. Given that the telogen HF relies in a close association between DP
612 and HG to efficiently induce the entry into the growing phase, DP displacement would lead cyst-bearing
613 HFs to become irreversibly telogen-arrested. Another possible additional mechanism would rely on the
614 altered cyst fate, unable to normally signal back to the bulge promoting stem cell self-renewal and anagen
615 entry, as happens when ORS and TACs are generated during the normal hair growth phase [21, 22].

616 These cumulative alterations triggered by cyst growth would have long-term consequences in bulge
617 homeostasis and architecture. Changes in ECM properties and HFSC niche structural perturbations have
618 been described to impact SC self-renewal in the context of aging, potentially connecting to HFSC loss [49,
619 81-83]. Compared to control mice, GRK2 eKO mice no longer show distinction between outer and inner
620 bulge cell layers, with abnormal distribution of markers such as of E- and P-cadherins, ZO-1, β-catenin or
621 F-actin, supporting the hypothesis of an aberrant organization of both cell layers affecting their functionality
622 [84]. Such bulge structural aberrations progress from 8 to 18M, with unstructured HFSC clusters
623 progressively lowering their CD34 levels, eventually leading to an unrecognizable bulge structure located
624 below the sebaceous gland in aged mice. Thus, we postulated that the more hair cycles take place as mouse
625 age, the more HFs would be transformed into cysts, hindering DP-bulge interactions and bulge functionality,
626 and driving the hair loss phenotype in GRK2 eKO animals. Consistent with this notion, repetitive depilation
627 exacerbates stem cell exhaustion and bulge destruction concomitant with macroscopic hair loss in GRK2
628 eKO mice.

629 Curiously, cysts emergence is not linked to development of spontaneous tumors with aging in GRK2 eKO
630 mice, despite persistent lineage infidelity and several tumoral markers in basal conditions, reminiscent to
631 that observed during wound healing or epithelial tumorigenesis [18], suggesting the existence of
632 compensatory or counteracting processes. We find that GRK2 eKO cysts are destroyed during aging by
633 mechanisms resembling those operating in immune-mediated alopecias.

634 The hair follicle bulge is known to be an immune-privileged site to avoid damaging long-lasting stem cells
635 or its transient progeny [51, 53, 85]. The loss of such immune privilege is associated with different types of
636 immune-mediated hair disorders, as alopecia areata (AA) or primary cicatricial alopecia (PCA), depending
637 on the HF compartment displaying a collapsed privilege. Strikingly, key histological similarities are found
638 between GRK2 eKO phenotype and AA, namely perifollicular $CD4^+$ T-cells ("swarm of bees"), ICAM1
639 expression, the presence of dystrophic hairs ("exclamation point hairs"), or pigmentary incontinence. Similar
640 to AA pathological mechanisms, bulge cells seem to be spared from immune-mediated destruction in our
641 model. However, the main inflammatory targets differ between AA and GRK2 eKO mice, since the
642 lymphocytic infiltration concentrates around HF-derived cysts rather than in the anagen HF proximal bulb.

643 Despite such differences in pathogenic processes, we have observed a significant correlation at the
644 transcriptional level between whole skin GRK2 eKO RNA expression patterns and the ones present in AA
645 patients during disease onset. Interestingly, cyst emergence can attract both intraepithelial and peripheral
646 $CD45^+$ cells even in the presence of an intact basal layer, owing to its intrinsic chemoattractant ability, which
647 might be potentiated when immunogenic keratinocyte and melanocyte-derived peptides are released to the
648 dermis once the basement membrane is discontinued during cyst destruction [52, 86], eventually leading to
649 foreign body giant cell formation.

650 In the context of HF cells, lineage infidelity has been described to impact long-term hair homeostasis via
651 triggering immune-mediated bulge cell destruction both in mouse models and human PCA follicular samples
652 [87]. It is tempting to postulate that in our mouse model mixed fate cyst emergence triggers an immune-
653 mediated attack, and that loss of immune privilege secondary to lineage infidelity might mechanistically
654 explain AA proximal bulb apoptosis. Thus, our model points to long-term lineage infidelity and its
655 association with stress-induced states as a major player in this process.

656 In sum, our work identifies keratinocyte GRK2 as a key player in HF homeostasis, cycling features and cell
657 fate determination. Our data provide a better understanding on how abnormal HF-committed cells develop
658 dystrophic follicular cysts and, on the mechanisms, linking cyst formation with hair loss, as well as suggest
659 potentially interesting connections among these processes and the pathogenic mechanisms operating in
660 immune-mediated alopecias. Further investigations are required to deepen in such connections and the
661 underlying molecular mechanisms, and to explore the potential role of keratinocyte GRK2 in skin
662 interfollicular homeostasis.

663
664
665 ## Methods
666
667 **Experimental design.** The objective of this study was to investigate the role of the GRK2 signaling hub in
668 hair follicle biology. For this purpose, we have generated a mouse model with specific deletion of this kinase
669 in keratinocytes and performed a thorough phenotypic and molecular characterization of these animals using
670 a combination of histological, imaging and molecular biology approaches described in this section.
671
672 **Animal protocols.** Mouse models used for these studies were housed and bred following all established
673 regulatory standards, and all the experiments were performed in accordance to guidelines of the
674 European Convention for the Protection of Vertebrate Animals used for Experimental and Other
675 Scientific Purposes (Directive 86/609/EEC) and with the authorization of the Bioethical Committee of
676 the Universidad Autónoma de Madrid and the Local Government (PROEX 339/14 and 118.8/21). The
677 animal research facility of the CBMSO has the appropriate license to hold and use animals for scientific
678 research (ES280790000180).
679 All the animals were bred and housed on a 12-hour light/dark cycle with free access to food and water. They
680 were maintained at a room temperature of 22±2 ºC with a relative humidity of 50±10% and under pathogen-
681 free conditions.
682 <u>*GRK2$^{F/F}$;K14-Cre* mice</u>. The C57BL/6 mouse strain carrying targeted GRK2 deletion in stratified epithelia
683 was generated by crossing mouse expressing the Cre recombinase under the human Keratin 14 promoter
684 (*K14-Cre*) [88, 89] with our mouse bearing GRK2 floxed alleles ($GRK2^{F/F}$) [90]. The resulting hemizygous
685 Cre positive males from this generation (F1) was then crossed to Cre negative hemizygous females to obtain
686 a mixture of Cre positive and negative with floxed GRK2 in homozygosity (F2), which were then used for
687 experiments and termed as GRK2 eKO.
688 <u>Tamoxifen-induced GRK2 knockout mice</u> were generated by crossing floxed GRK2 (*Grk2$^{F/F}$*) mice with
689 TxCre animals (from Dr. A. Kavelaars, University Medical Center Utrecht, Utrecht, the Netherlands), in

690 which Cre recombinase expression is induced by the administration of tamoxifen. Floxed homozygous
691 GRK2 mice (*Grk2*$^{F/F}$) [72] and transgenic mice overexpressing a Cre recombinase fused to a mutant form
692 of the estrogen receptor (ER) to allow for tamoxifen-dependent activation [B6.Cg-Tg(CAG-
693 cre/Esr1*)5Amc/J] [91] were obtained from The Jackson Laboratory. *Cre*$^{+/-}$*Grk2*$^{F/wt}$ offsprings were
694 backcrossed with *GRK2*$^{F/F}$ mice to obtain mice carrying both floxed GRK2 alleles and, either none
695 (*Cre*$^{-/-}$*;Grk2*$^{F/F}$) or a single CreER allele (*Cre*$^{+/-}$*;Grk2*$^{F/F}$).
696 For the experimental procedure, 2-month-old *Tx-CreGrk2*$^{F/F}$ mice were injected with 2 mg of tamoxifen
697 (#T2859, Sigma Aldrich) in corn oil (#C8267, Sigma Aldrich) for 5 consecutive days to induce GRK2
698 depletion.
699 For mouse genotyping, genomic DNA extraction was performed by lysing a fragment of mouse tail in a lysis
700 buffer containing EDTA (#E9884, Sigma Aldrich), SDS (CBMSO facility) and Proteinase K (#EO0491,
701 Thermo Fisher) and using 2-propanol and ethanol (Merck) to precipitate the DNA. Then, mice were
702 genotyped by using two different specific primers for PCR to detect either Cre (5'-
703 CGATGCAACGAGTGATGAGGTTC-3'; 5'-GCACGTTCACCGGCATCAAC-3') or GRK2 floxed
704 alleles (5'-TGAGGCTCAGGGATACCTGTCAT-3'; 5'-GTTAGCTCAGGCCAACAAGCC-3'; 5'-
705 CAGGCATTCCTGCTGGACTAG-3'). The products of amplification with the DNA dye as loading buffer
706 6X (#N472, EZVISION®) were subjected to electrophoresis on a 1-3.5% agarose gel in TAE and the
707 resulting bands were detected using ultraviolet light.
708
709 **In vivo protocols.** For proliferation analysis, BrdU (Roche) was injected intraperitoneally to mice at 0.1
710 mg/g weight in 0.9% NaCl 2 hours before sacrifice.
711 Recombination in *TxCre-Grk2*$^{F/F}$ mice was induced by an intraperitoneal injection of tamoxifen (Sigma-
712 Aldrich, 2 mg per mouse, in 0.9% NaCl, containing 9% ethanol and 51% sunflower oil), for five consecutive
713 days. For depilation experiments, synchronized back skin mouse was used. Hair was removed with an
714 electric razor and then, Veet depilatory cream was applied for 1 min. For repetitive depilation experiments,
715 this process was repeated every month, up to a total of 9 times.
716
717 **Histological procedures**
718 Immunohistochemistry and immunofluorescence. After tissue harvesting, skin was fixed in 10% neutral
719 buffered formalin (#HT501128, Sigma Aldrich) for 24h, then paraffin embedded and 5 µm thick sections
720 were used for Hematoxylin (#7211, Thermo Scientific) and Eosin (#HT110332, Sigma Aldrich) staining
721 (H&E), following conventional protocols described elsewhere. The rest of the tissue was embedded unfixed
722 in OCT (Optimal cutting temperature) compound (#4583, Sakura) and frozen using dry ice.
723 Immunohistochemistry of paraffin-embedded (FPPE) sections was performed following standard protocols
724 with citrate buffer-mediated antigen retrieval and using biotin-conjugated secondary antibodies, Vectastain®
725 ABC kit (#PK-4000, Vector laboratories) for peroxidase signal amplification and DAB (#SK-4100, Vector
726 laboratories) for antigen visualization. Sections were then counterstained with hematoxylin and mounted in
727 Sub-X mounting medium (#3801740, Leica).
728 Fontana-Masson melanin staining. For melanin staining, OCT tissue samples were sectioned at 12 µm
729 thickness, with the use of a cryostat (#CM1950, Leica), and stained with the Fontana-Masson kit (#HT200-
730 1KT, Sigma), following the manufacturer instructions.
731 Horizontal whole mount. For complete hair follicle visualization, immunofluorescence staining was
732 performed on thick OCT sections (60-70 µm). Briefly, horizontal whole mount sections were fixed for 15
733 mins in 4% paraformaldehyde (#30525-89-4, Santa Cruz Biotechnology) in PBS, permeabilized for 10
734 minutes with 0.1% Triton X-100 (#X100, Sigma) in PBS, and blocked for 1 hour in PBS containing 0.05%
735 Triton X-100, 1% Gelatin from cold water fish skin (#G7041, Sigma), 1,5% BSA (#3117332001, Roche)
736 and 1,5% of donkey serum (#D9663, Sigma). Sections were incubated with primary antibodies (see table)
737 overnight at 4ºC, rinsed with PBS and incubated with secondary antibodies (see table) during 4h at room

temperature, counterstained with DAPI (CBMSO microscopy facility) and mounted in Mowiol (CBMSO microscopy facility).

Proliferation assay. To detect BrdU incorporation the immunofluorescence protocol was modified, and permeabilization step was followed by 15 min incubation with HCl 2N at room temperature.

Lipid staining. For Nile Red staining, OCT sections (12 µm thick) were fixed for 5 min with paraformaldehyde, then incubated with Nile Red (#19123, Sigma Aldrich) at 2 µg/ml for 30 min, rinsed, counterstained with DAPI and visualized with the corresponding red fluorescence filter.

Apoptosis determination via TUNEL. Terminal deoxynucleotidyl transferase dUTP nick end labeling (TUNEL) (#12156792910, Roche) staining protocol was performed according to the manufacturer instructions. Briefly, 5 µm paraffin-embedded sections were deparaffinized, then the antigen retrieval was performed with citrate buffer pH 6, followed by incubation with the reaction mix with the label and enzyme solutions for 1 hour at 37ºC and counterstained with DAPI.

RNA sequencing and analysis. Total RNA from dorsal mouse skin was isolated from 5 control and 5 transgenic GRK2 eKO animals with RNAEasy Mini kit (#74104, Qiagen), following manufacturer instructions. Upon collection, skin was incubated overnight at 4ºC with RNA Later solution (#10391085, Invitrogen) and then stored at -80ºC. RNA-preserved tissue was thawed, and 20 mg were homogenized using metal beads with Tissue Lyser (Qiagen) in QIAzol solution (#79306, Qiagen). To avoid genomic DNA contamination, DNA digestion was performed in column with RNase-free DNaseI (#79254, Qiagen). RNA samples with RIN > 8 were used. RNA sequencing was performed after poly-A selection using Illumina NovaSeq 2x150 bp sequencing. Reads were aligned to GRCm39 mouse genome with "Rbowtie2", counts extracted with featureCounts function from "Rsubread" and Gencode annotation release 27 (gencode.vM27.annotation.gtf). Raw and processed data are deposited at the GEO database under the accession GSE261821.

Differential expression between skin from control and GRK2 eKO animals was performed using DESeq2. We consider genes significantly over- or under-expressed if they had p-val<0.05 and adjusted pval<0.25. Gene Set Enrichment Analysis (https://www.gsea-msigdb.org/gsea/index.jsp) was used to analyze enrichment of genesets in transcriptome datasets. GSEA from RNA-seq was performed from DESeq2 normalized counts after removal of genes with counts=0 in all samples. Genesets were retrieved from MSigDB signature database (https://www.gsea-msigdb.org/gsea/msigdb/index.jsp) or were generated from in-house analyses. The "GRK2 eKO signature" used in Figure AA was constituted by 231 genes significantly overexpressed in the skin of GRK2 eKO mice when compared to Control animals, upon DESeq2 analysis (see above). The "Human AA signature" in Figure AA was composed of 353 genes overexpressed in AA samples (patchy type and transient patchy type samples) when compared with non-affected skin, upon Ttest analysis of the AA dataset GSE45513 retrieved from Gene Expression Omnibus (GEO) database (PMID: 27322477). Functional analyses were additionally performed with the ToppFun utility from the TopGene Suite (https://toppgene.cchmc.org/). Heatmap of individual genes was represented using MeV software (https://doi.org/10.1007/978-1-4419-5714-6_15). Graphical representation of selected GSEA was performed using ggplot2 in R [92].

Data and materials availability. Raw and processed data are deposited at the GEO database under the accession GSE261821.

Flow cytometry. For the preparation of a cell suspension of keratinocytes from the back skin, first, subcutaneous fat was removed using a scalpel. Afterwards, the epidermis was placed, side up, into a p100 dish with 0.25% trypsin solution (generated at our cell culture facility) and cultured overnight at 4ºC. Epidermis was scraped and filtered through 70 and 40 µm cell strainers (Falcon) to obtain the single cell suspension by centrifugation. To sort the target cells, the cell suspension obtained was stained with CD34-

786 eFluor660 and integrin a6 (CD49f)-FITC, for 1h at 4ºC, in a buffer containing 2% FBS in PBS using a
787 FACSAria Fusion (BSC II) device. Dead cells were excluded with the use of propidium iodide (#P4170,
788 Sigma).
789
790 **Protein extract preparation and Western Blot.** 2-month-old mouse epidermal single cell suspension was
791 pelleted and lysed in Laemli lysis buffer and protease (62.5 mM Tris base pH 7.4, 2% SDS (v/v), 10%
792 glicerol (v/v)) and phosphatase inhibitor cocktail (#87785, Thermo Scientific).
793 Protein samples were mixed with 4X loading buffer, boiled for 5 min at 95ºC and resolved by SDS-PAGE
794 in 4–15% Mini-PROTEAN® TGX™ Precast Protein Gels (#4561086, BioRad). After electrophoresis,
795 proteins were transferred to 0.45 µm nitrocellulose membranes (#1620115, BioRad) and then stained with
796 Ponceau S (#141194, Sigma Aldrich). Membranes were blocked using 5% BSA (#3117332001, Roche) in
797 TBS pH 8 buffer solution, and incubated overnight with primary antibodies (see table). Membranes were
798 then washed with 0.1% Tween-20 TBS solution (#8221840050, Sigma Aldrich) and incubated with HRP-
799 conjugated secondary antibody at room temperature for 1h. Membrane-bound secondary antibody was
800 detected using Western Lightning ECL Plus (#NEL103E001EA, Perkin Elmer) and Medical X-Ray blue
801 films (#FA158, Agfa). The bands were quantified by laser densitometry with a Biorad GS-700 scanner.
802
803 **Electron microscopy.** Skin samples were fixed with 4% paraformaldehyde (Santa Cruz Biotechnology) and
804 2% glutaraldehyde (Sigma) in 0.1M phosphate buffer pH 7.4, for 2 h at room temperature and overnight at
805 4º C. Samples were rinsed with PBS and postfixed with 1% osmium tetroxide (Sigma) and 0.8% Potassium
806 Ferricianyde (Sigma) in bidistilled water, at 4 °C for 1 h, then incubated with 0.15% tanic (Sigma) acid for
807 1 min at room temperature. After several washes, skins were incubated with 2% uranyl acetate (Sigma), for
808 1 h at room temperature, and dehydrated in a graded series of ethanol (Merck).
809 Infiltration of the resin was accomplished by incubating the samples in a mixture of ethanol and propylene
810 oxide (#540021, Sigma Aldrich) 1:1 (V:V), for 5 min at room temperature followed by incubations in
811 propylene oxide 10 min at RT. Then, the samples were incubated, for 45 min at RT, in a mixture (1:1; V:V)
812 of propylene oxide and epoxi resin (#TAAB 812 , TAAB Laboratories). Finally, the samples were incubated
813 1hr, at room temperature and overnight, in pure resin under agitation, and the next day incubated for 3h into
814 renewed resin and placed into flat embedding molds. Polymerization of infiltrated samples was done at 60ºC
815 for 2 days.
816 Ultrathin sections of 70-80 nm were cut with an ultramicrotome Ultracut E (Leica) and mounted on Formvar-
817 carbon-coated Cu/Pd 100-mesh or slot grids. Next, they were stained with uranyl acetate and lead citrate. A
818 JEM1400 Flash (Jeol) transmission electron microscope was used at 100 kV, with a Oneview 4K x4K CMOS
819 camera (Gatan).
820
821 **Microscopy.** Fluorescence images were acquired with Zeiss confocal microscopes (Inverted LSM 700,
822 Inverted LSM 800 or Vertical LSM 900). For widefield color images vertical AxioImager M1 coupled with
823 a camera DMC6200 (Leica) was used. Image acquisition and processing was performed with the use of Zen
824 software (Carl Zeiss) and Fiji (ImageJ).
825
826 **Statistics.** Data is represented as mean values ± SEM of the indicated number of mice in the figure legend.
827 Statistical significance has been determined using GraphPad Prism 8 software by two-sided unpaired
828 Student's t-test, for one-to-one comparisons, and by one-way ANOVA followed by the Bonferroni's test in
829 the case of multiple mean comparisons. Statistical significance as well as n is specified in each figure legend
830
831
832
833

834 **Table 1.** List of antibodies used.

835

Target	Source	Ref.	Use	Dilution
GRK2	Novus	NBP1-32534	IHQ	1/250
GRK2	Abcam	137666	WB	1/1500
β-Actin	Sigma	A5441	WB	1/1000
α6 integrin/CD49f-conj	Invitrogen	11-0495-82	IF, FACS	1/100
Sox9	Sigma	AB5535	IF	1/400
Keratin 15	Thermo Fisher	MS-1068	IF	1/300
CD34	Abcam	ab81289	IF	1/400
P-cadherin	R&D Systems	AF761	IF	1/200
Ki67	Thermo Fisher	RM-9106-S	IF	1/300
CD34-eFluor (660)	Invitrogen	50-0341-80	IF, FACS	1/100
BrdU	Abcam	6326	IF	1/250
Lef1	Cell Signaling	2230	IF	1/100
βCatenin	BD Biosciences	610154	IF	1/200
GRK2	In house		IF	1/400
Lrig1	R&D Systems	AF3688-SP	IF	1/100
Keratin 5	Convance	PRB-160P	IF	1/400
Keratin 6	Covance	905701	IF	1/400
CDP	Proteintech	11733-1-AP	IF	1/100
Gata3	Invitrogen	14-9966-82	IF	1/100
Klf5	R&D Systems	AF3758-SP	IF	1/50
ΔNp63	Biolegend	Poly6190	IF	1/150
cJun	Cell Signaling	9165	IF	1/100
Tenascin C	Sigma	T3413	IF	1/200
αSMA	Dako	M0851	IF	1/50
Gata6	Cell Signaling	5851	IF	1/250
Filaggrin	Covance	PRB-417P	IF	1/400
Keratin 10	Dako	M 7002	IF	1/100
Loricrin	Covance	PRB-145P	IF	1/400
ZO-1	Invitrogen	40-2200	IF	1/100
E-Cadherin	Cell Signaling	3195	IF	1/300
Faloidin Alexa Fluor 555	Thermo Fisher	A34055	IF	1/100
CD45	Life Technologies	14-0451	IF	1/250
Y-H2AX	Cell Signaling	9718	IF	1/150
Cleaved Caspase 3	Cell Signaling	9661L	IF	1/100
CD3	Biolegend	100201	IF	1/200
ICAM1	R&D Systems	AF796	IHQ	1/100
MHC-II (I-A/I-E)	Biolegend	107601	IF	1/200
F4/80	Abcam	16911	IF	1/70
Goat anti Rabbit IgG conjugated with Horseradish peroxidase	Nordicmubio	GAR/IgG(H+L)/PO	WB	1/50000
Goat anti Mouse IgG1 IgG2a IgG2b IgG3 conjugated with Horseradish peroxidase	Nordicmubio	GAM/IgG(H+L)/PO	WB	1/50000
Biotin-SP AffiniPure Donkey Anti-Goat IgG (H+L)	Jackson Immunoresearch	705-065-147	IHQ	1/3000
Biotin-SP AffiniPure Donkey Anti-Rabbit IgG (H+L)	Jackson Immunoresearch	711-065-152	IHQ	1/3000
Alexa 488 Donkey anti-Goat IgG	Thermo Fisher	A-11055	IF	1/250

Alexa 488 Donkey anti-Mouse IgG	Thermo Fisher	A-21202	IF	1/250
Alexa 488 Donkey anti-Rabbit IgG	Thermo Fisher	A-21206	IF	1/250
Alexa 555 Donkey anti-Goat IgG	Thermo Fisher	A-21432	IF	1/250
Alexa 555 Donkey anti-Mouse IgG	Thermo Fisher	A-31570	IF	1/250
Alexa 555 Donkey anti-Rabbit IgG	Thermo Fisher	A-31572	IF	1/250
Alexa 647 Donkey anti-Goat IgG	Thermo Fisher	A-21447	IF	1/250
Alexa 647 Donkey anti-Mouse IgG	Thermo Fisher	A-31571	IF	1/250
Alexa 647 Donkey anti-Rabbit IgG	Thermo Fisher	A-31573	IF	1/250

Competing interests

The authors declare no competing interests.

Acknowledgments

We thank Prof. Fiona M. Watt (EMBL Heidelberg) for her guidance during Alejandro Asensio´s training at King's College London in the initial stages of this work. We thank Cristina Delgado and Estefanía Vázquez Oro for their helpful technical assistance, and Pilar Hernández, Angustias Page and Carmen Segrelles for their excellent assistance with the histological processing of the samples at CIEMAT histology facility. The help from CBMSO Animal Care, Flow Cytometry, Electron and Optical and Confocal Microscopy facilities is also acknowledged.

This work was supported by:
Agencia Estatal de Investigación of Spain (grant PID2020-117218RB-I00 to FM)
(H2020-MSCA Program, Grant agreement 860229-ONCORNET 2.0 to FM)
CIBERCV-Instituto de Salud Carlos III, Spain (grant CB16/11/00278 to FM, co-funded with European FEDER contribution)
Fundación Ramón Areces (to FM and CR)
Instituto de Salud Carlos III (grant PI22_00966 to C.R., co-funded with European FEDER contribution)
Programa de Actividades en Biomedicina de la Comunidad de Madrid- S2022/BMD-7209 - INTEGRAMUNE (to FM)
AA held a PhD Fellowship from FPI programme Agencia Estatal de Investigación (PRE2018-084418)
We also acknowledge institutional support to the CBM from Fundación Ramón Areces.

Author contributions

AA designed and performed experiments, prepared figures, analyzed data, wrote and revised manuscript; MSF, JPG performed some experiments, analyzed data and prepared figures; KLA and JMP helped with study concepts and revised manuscript, RGE performed functional genomic analysis, provided study concepts, wrote and revised manuscript; FM Jr, and CR provided study concept and design, interpreted experiments, supervised the study, wrote and revised manuscript and obtained funding.

Competing interests

The authors declare no competing interests.

References

877 1. Foitzik, K., et al., *Control of murine hair follicle regression (catagen) by TGF-beta1 in*
878 *vivo.* Faseb j, 2000. **14**(5): p. 752-60.
879 2. Schneider, M.R., R. Schmidt-Ullrich, and R. Paus, *The hair follicle as a dynamic*
880 *miniorgan.* Curr Biol, 2009. **19**(3): p. R132-42.
881 3. Müller-Röver, S., et al., *A comprehensive guide for the accurate classification of murine*
882 *hair follicles in distinct hair cycle stages.* J Invest Dermatol, 2001. **117**(1): p. 3-15.
883 4. Hsu, Y.C., H.A. Pasolli, and E. Fuchs, *Dynamics between stem cells, niche, and progeny*
884 *in the hair follicle.* Cell, 2011. **144**(1): p. 92-105.
885 5. Phillips, T.G., W.P. Slomiany, and R. Allison, *Hair Loss: Common Causes and*
886 *Treatment.* Am Fam Physician, 2017. **96**(6): p. 371-378.
887 6. Blanpain, C., et al., *Self-renewal, multipotency, and the existence of two cell populations*
888 *within an epithelial stem cell niche.* Cell, 2004. **118**(5): p. 635-48.
889 7. Schepeler, T., M.E. Page, and K.B. Jensen, *Heterogeneity and plasticity of epidermal stem*
890 *cells.* Development, 2014. **141**(13): p. 2559-67.
891 8. Ito, M., et al., *Hair follicle stem cells in the lower bulge form the secondary germ, a*
892 *biochemically distinct but functionally equivalent progenitor cell population, at the*
893 *termination of catagen.* Differentiation, 2004. **72**(9-10): p. 548-57.
894 9. Morgan, B.A., *The dermal papilla: an instructive niche for epithelial stem and progenitor*
895 *cells in development and regeneration of the hair follicle.* Cold Spring Harb Perspect Med,
896 2014. **4**(7): p. a015180.
897 10. Horne, K.A., C.A. Jahoda, and R.F. Oliver, *Whisker growth induced by implantation of*
898 *cultured vibrissa dermal papilla cells in the adult rat.* J Embryol Exp Morphol, 1986. **97**:
899 p. 111-24.
900 11. Jahoda, C.A., K.A. Horne, and R.F. Oliver, *Induction of hair growth by implantation of*
901 *cultured dermal papilla cells.* Nature, 1984. **311**(5986): p. 560-2.
902 12. Link, R.E., et al., *Epithelial growth by rat vibrissae follicles in vitro requires*
903 *mesenchymal contact via native extracellular matrix.* J Invest Dermatol, 1990. **95**(2): p.
904 202-7.
905 13. Mesa, K.R., P. Rompolas, and V. Greco, *The Dynamic Duo: Niche/Stem Cell*
906 *Interdependency.* Stem Cell Reports, 2015. **4**(6): p. 961-6.
907 14. Rompolas, P., et al., *Live imaging of stem cell and progeny behaviour in physiological*
908 *hair-follicle regeneration.* Nature, 2012. **487**(7408): p. 496-9.
909 15. Yang, H., et al., *Epithelial-Mesenchymal Micro-niches Govern Stem Cell Lineage*
910 *Choices.* Cell, 2017. **169**(3): p. 483-496.e13.
911 16. Greco, V., et al., *A two-step mechanism for stem cell activation during hair regeneration.*
912 Cell Stem Cell, 2009. **4**(2): p. 155-69.
913 17. Adam, R.C., et al., *Temporal Layering of Signaling Effectors Drives Chromatin*
914 *Remodeling during Hair Follicle Stem Cell Lineage Progression.* Cell Stem Cell, 2018.
915 **22**(3): p. 398-413.e7.
916 18. Ge, Y., et al., *Stem Cell Lineage Infidelity Drives Wound Repair and Cancer.* Cell, 2017.
917 **169**(4): p. 636-650.e14.
918 19. Vauclair, S., et al., *Notch1 is essential for postnatal hair follicle development and*
919 *homeostasis.* Dev Biol, 2005. **284**(1): p. 184-93.
920 20. Watt, F.M., S. Estrach, and C.A. Ambler, *Epidermal Notch signalling: differentiation,*
921 *cancer and adhesion.* Curr Opin Cell Biol, 2008. **20**(2): p. 171-9.
922 21. Hsu, Y.C., L. Li, and E. Fuchs, *Transit-amplifying cells orchestrate stem cell activity and*
923 *tissue regeneration.* Cell, 2014. **157**(4): p. 935-49.
924 22. Jaks, V., et al., *Lgr5 marks cycling, yet long-lived, hair follicle stem cells.* Nat Genet,
925 2008. **40**(11): p. 1291-9.

926 23. Genander, M., et al., *BMP signaling and its pSMAD1/5 target genes differentially regulate*
927 *hair follicle stem cell lineages.* Cell Stem Cell, 2014. **15**(5): p. 619-33.
928 24. Oshimori, N. and E. Fuchs, *Paracrine TGF-β signaling counterbalances BMP-mediated*
929 *repression in hair follicle stem cell activation.* Cell Stem Cell, 2012. **10**(1): p. 63-75.
930 25. Zhang, J., et al., *Bone morphogenetic protein signaling inhibits hair follicle anagen*
931 *induction by restricting epithelial stem/progenitor cell activation and expansion.* Stem
932 Cells, 2006. **24**(12): p. 2826-39.
933 26. Daszczuk, P., et al., *An Intrinsic Oscillation of Gene Networks Inside Hair Follicle Stem*
934 *Cells: An Additional Layer That Can Modulate Hair Stem Cell Activities.* Front Cell Dev
935 Biol, 2020. **8**: p. 595178.
936 27. Merrill, B.J., et al., *Tcf3 and Lef1 regulate lineage differentiation of multipotent stem cells*
937 *in skin.* Genes Dev, 2001. **15**(13): p. 1688-705.
938 28. Niemann, C., et al., *Expression of DeltaNLef1 in mouse epidermis results in differentiation*
939 *of hair follicles into squamous epidermal cysts and formation of skin tumours.*
940 Development, 2002. **129**(1): p. 95-109.
941 29. Lowry, W.E., et al., *Defining the impact of beta-catenin/Tcf transactivation on epithelial*
942 *stem cells.* Genes Dev, 2005. **19**(13): p. 1596-611.
943 30. DasGupta, R. and E. Fuchs, *Multiple roles for activated LEF/TCF transcription complexes*
944 *during hair follicle development and differentiation.* Development, 1999. **126**(20): p.
945 4557-68.
946 31. Lien, W.H., et al., *In vivo transcriptional governance of hair follicle stem cells by*
947 *canonical Wnt regulators.* Nat Cell Biol, 2014. **16**(2): p. 179-90.
948 32. Mesler, A.L., et al., *Hair Follicle Terminal Differentiation Is Orchestrated by Distinct*
949 *Early and Late Matrix Progenitors.* Cell Rep, 2017. **19**(4): p. 809-821.
950 33. Yamamoto, N., et al., *Notch/RBP-J signaling regulates epidermis/hair fate determination*
951 *of hair follicular stem cells.* Curr Biol, 2003. **13**(4): p. 333-8.
952 34. Yuhki, M., et al., *BMPR1A signaling is necessary for hair follicle cycling and hair shaft*
953 *differentiation in mice.* Development, 2004. **131**(8): p. 1825-33.
954 35. Kobielak, K., et al., *Loss of a quiescent niche but not follicle stem cells in the absence of*
955 *bone morphogenetic protein signaling.* Proc Natl Acad Sci U S A, 2007. **104**(24): p.
956 10063-8.
957 36. Demehri, S. and R. Kopan, *Notch signaling in bulge stem cells is not required for*
958 *selection of hair follicle fate.* Development, 2009. **136**(6): p. 891-6.
959 37. Qiu, W., et al., *Conditional activin receptor type 1B (Acvr1b) knockout mice reveal hair*
960 *loss abnormality.* J Invest Dermatol, 2011. **131**(5): p. 1067-76.
961 38. Kadaja, M., et al., *SOX9: a stem cell transcriptional regulator of secreted niche signaling*
962 *factors.* Genes Dev, 2014. **28**(4): p. 328-41.
963 39. White, A.C., et al., *Stem cell quiescence acts as a tumour suppressor in squamous*
964 *tumours.* Nat Cell Biol, 2014. **16**(1): p. 99-107.
965 40. Penela, P., et al., *The complex G protein-coupled receptor kinase 2 (GRK2) interactome*
966 *unveils new physiopathological targets.* Br J Pharmacol, 2010. **160**(4): p. 821-32.
967 41. Ranjan, R., et al., *Novel Structural Insights into GPCR-β-Arrestin Interaction and*
968 *Signaling.* Trends Cell Biol, 2017. **27**(11): p. 851-862.
969 42. Nogués, L., et al., *G protein-coupled receptor kinases (GRKs) in tumorigenesis and*
970 *cancer progression: GPCR regulators and signaling hubs.* Semin Cancer Biol, 2018. **48**:
971 p. 78-90.
972 43. Palacios-García, J., et al., *G-protein-coupled receptor kinase 2 safeguards epithelial*
973 *phenotype in head and neck squamous cell carcinomas.* Int J Cancer, 2020. **147**(1): p.
974 218-229.

975 44. Wang, Q., et al., *A multi-scale model for hair follicles reveals heterogeneous domains*
976 *driving rapid spatiotemporal hair growth patterning.* Elife, 2017. **6**.
977 45. Joost, S., et al., *Single-Cell Transcriptomics Reveals that Differentiation and Spatial*
978 *Signatures Shape Epidermal and Hair Follicle Heterogeneity.* Cell Syst, 2016. **3**(3): p.
979 221-237.e9.
980 46. Biehs, B., et al., *A cell identity switch allows residual BCC to survive Hedgehog pathway*
981 *inhibition.* Nature, 2018. **562**(7727): p. 429-433.
982 47. Li, L. and H. Clevers, *Coexistence of quiescent and active adult stem cells in mammals.*
983 Science, 2010. **327**(5965): p. 542-5.
984 48. Lay, K., T. Kume, and E. Fuchs, *FOXC1 maintains the hair follicle stem cell niche and*
985 *governs stem cell quiescence to preserve long-term tissue-regenerating potential.* Proc
986 Natl Acad Sci U S A, 2016. **113**(11): p. E1506-15.
987 49. Fuchs, E. and H.M. Blau, *Tissue Stem Cells: Architects of Their Niches.* Cell Stem Cell,
988 2020. **27**(4): p. 532-556.
989 50. Tumeh, P.C., et al., *PD-1 blockade induces responses by inhibiting adaptive immune*
990 *resistance.* Nature, 2014. **515**(7528): p. 568-71.
991 51. Paus, R., B.J. Nickoloff, and T. Ito, *A 'hairy' privilege.* Trends Immunol, 2005. **26**(1): p.
992 32-40.
993 52. Bertolini, M., et al., *Hair follicle immune privilege and its collapse in alopecia areata.*
994 Exp Dermatol, 2020. **29**(8): p. 703-725.
995 53. Gilhar, A., R. Paus, and R.S. Kalish, *Lymphocytes, neuropeptides, and genes involved in*
996 *alopecia areata.* J Clin Invest, 2007. **117**(8): p. 2019-27.
997 54. Messenger, A.G., D.N. Slater, and S.S. Bleehen, *Alopecia areata: alterations in the hair*
998 *growth cycle and correlation with the follicular pathology.* Br J Dermatol, 1986. **114**(3):
999 p. 337-47.
1000 55. Pratt, C.H., et al., *Alopecia areata.* Nat Rev Dis Primers, 2017. **3**: p. 17011.
1001 56. Jabbari, A., et al., *Molecular signatures define alopecia areata subtypes and*
1002 *transcriptional biomarkers.* EBioMedicine, 2016. **7**: p. 240-7.
1003 57. Panteleyev, A.A., C.A. Jahoda, and A.M. Christiano, *Hair follicle predetermination.* J
1004 Cell Sci, 2001. **114**(Pt 19): p. 3419-31.
1005 58. Zhang, Y.V., et al., *Distinct self-renewal and differentiation phases in the niche of*
1006 *infrequently dividing hair follicle stem cells.* Cell Stem Cell, 2009. **5**(3): p. 267-78.
1007 59. Rompolas, P., K.R. Mesa, and V. Greco, *Spatial organization within a niche as a*
1008 *determinant of stem-cell fate.* Nature, 2013. **502**(7472): p. 513-8.
1009 60. Panteleyev, A.A., *Functional anatomy of the hair follicle: The Secondary Hair Germ.* Exp
1010 Dermatol, 2018. **27**(7): p. 701-720.
1011 61. Kaufman, C.K., et al., *GATA-3: an unexpected regulator of cell lineage determination in*
1012 *skin.* Genes Dev, 2003. **17**(17): p. 2108-22.
1013 62. Li, M., et al., *Skin abnormalities generated by temporally controlled RXRalpha mutations*
1014 *in mouse epidermis.* Nature, 2000. **407**(6804): p. 633-6.
1015 63. Li, M., et al., *RXR-alpha ablation in skin keratinocytes results in alopecia and epidermal*
1016 *alterations.* Development, 2001. **128**(5): p. 675-88.
1017 64. Ellis, T., et al., *The transcriptional repressor CDP (Cutl1) is essential for epithelial cell*
1018 *differentiation of the lung and the hair follicle.* Genes Dev, 2001. **15**(17): p. 2307-19.
1019 65. Hughes, M.W., et al., *Disrupted ectodermal organ morphogenesis in mice with a*
1020 *conditional histone deacetylase 1, 2 deletion in the epidermis.* J Invest Dermatol, 2014.
1021 **134**(1): p. 24-32.
1022 66. Mesa, K.R., et al., *Niche-induced cell death and epithelial phagocytosis regulate hair*
1023 *follicle stem cell pool.* Nature, 2015. **522**(7554): p. 94-7.

1024 67. Latil, M., et al., *Cell-Type-Specific Chromatin States Differentially Prime Squamous Cell*
1025 *Carcinoma Tumor-Initiating Cells for Epithelial to Mesenchymal Transition.* Cell Stem
1026 Cell, 2017. **20**(2): p. 191-204.e5.
1027 68. Zhou, P., et al., *Lymphoid enhancer factor 1 directs hair follicle patterning and epithelial*
1028 *cell fate.* Genes Dev, 1995. **9**(6): p. 700-13.
1029 69. Millar, S.E., *Molecular mechanisms regulating hair follicle development.* J Invest
1030 Dermatol, 2002. **118**(2): p. 216-25.
1031 70. Bosakova, M., et al., *Mutations in GRK2 cause Jeune syndrome by impairing Hedgehog*
1032 *and canonical Wnt signaling.* EMBO Mol Med, 2020. **12**(11): p. e11739.
1033 71. Ho, J., et al., *The G protein-coupled receptor kinase-2 is a TGFbeta-inducible antagonist*
1034 *of TGFbeta signal transduction.* Embo j, 2005. **24**(18): p. 3247-58.
1035 72. Rivas, V., et al., *Developmental and tumoral vascularization is regulated by G protein-*
1036 *coupled receptor kinase 2.* J Clin Invest, 2013. **123**(11): p. 4714-30.
1037 73. Romano, R.A., et al., *Abnormal hair follicle development and altered cell fate of follicular*
1038 *keratinocytes in transgenic mice expressing DeltaNp63alpha.* Development, 2010. **137**(9):
1039 p. 1431-9.
1040 74. Gatti, V., et al., *ΔNp63-Senataxin circuit controls keratinocyte differentiation by*
1041 *promoting the transcriptional termination of epidermal genes.* Proc Natl Acad Sci U S A,
1042 2022. **119**(10): p. e2104718119.
1043 75. Walker, M.F., et al., *GRK2 Kinases in the Primary Cilium Initiate SMOOTHENED-PKA*
1044 *Signaling in the Hedgehog Cascade.* bioRxiv, 2024.
1045 76. Happ, J.T., et al., *A PKA inhibitor motif within SMOOTHENED controls Hedgehog signal*
1046 *transduction.* Nat Struct Mol Biol, 2022. **29**(10): p. 990-999.
1047 77. Iglesias-Bartolome, R., et al., *Inactivation of a Gα(s)-PKA tumour suppressor pathway in*
1048 *skin stem cells initiates basal-cell carcinogenesis.* Nat Cell Biol, 2015. **17**(6): p. 793-803.
1049 78. Matsumura, H., et al., *Hair follicle aging is driven by transepidermal elimination of stem*
1050 *cells via COL17A1 proteolysis.* Science, 2016. **351**(6273): p. aad4395.
1051 79. Oshima, H., et al., *Morphogenesis and renewal of hair follicles from adult multipotent*
1052 *stem cells.* Cell, 2001. **104**(2): p. 233-45.
1053 80. Rendl, M., L. Polak, and E. Fuchs, *BMP signaling in dermal papilla cells is required for*
1054 *their hair follicle-inductive properties.* Genes Dev, 2008. **22**(4): p. 543-57.
1055 81. Ge, Y., et al., *The aging skin microenvironment dictates stem cell behavior.* Proc Natl
1056 Acad Sci U S A, 2020. **117**(10): p. 5339-5350.
1057 82. Folgueras, A.R., et al., *Architectural niche organization by LHX2 is linked to hair follicle*
1058 *stem cell function.* Cell Stem Cell, 2013. **13**(3): p. 314-27.
1059 83. Koester, J., et al., *Niche stiffening compromises hair follicle stem cell potential during*
1060 *ageing by reducing bivalent promoter accessibility.* Nat Cell Biol, 2021. **23**(7): p. 771-
1061 781.
1062 84. Lay, K., et al., *Stem cells repurpose proliferation to contain a breach in their niche*
1063 *barrier.* Elife, 2018. **7**.
1064 85. Müller-Röver, S., et al., *Intercellular adhesion molecule-1 and hair follicle regression.* J
1065 Histochem Cytochem, 2000. **48**(4): p. 557-68.
1066 86. Wang, E.H.C., et al., *Identification of Autoantigen Epitopes in Alopecia Areata.* J Invest
1067 Dermatol, 2016. **136**(8): p. 1617-1626.
1068 87. Adam, R.C., et al., *NFI transcription factors provide chromatin access to maintain stem*
1069 *cell identity while preventing unintended lineage fate choices.* Nat Cell Biol, 2020. **22**(6):
1070 p. 640-650.
1071 88. Martínez-Cruz, A.B., et al., *Spontaneous squamous cell carcinoma induced by the somatic*
1072 *inactivation of retinoblastoma and Trp53 tumor suppressors.* Cancer Res, 2008. **68**(3): p.
1073 683-92.

89. Jonkers, J., et al., *Synergistic tumor suppressor activity of BRCA2 and p53 in a conditional mouse model for breast cancer.* Nat Genet, 2001. **29**(4): p. 418-25.
90. Matkovich, S.J., et al., *Cardiac-specific ablation of G-protein receptor kinase 2 redefines its roles in heart development and beta-adrenergic signaling.* Circ Res, 2006. **99**(9): p. 996-1003.
91. Hayashi, S. and A.P. McMahon, *Efficient recombination in diverse tissues by a tamoxifen-inducible form of Cre: a tool for temporally regulated gene activation/inactivation in the mouse.* Dev Biol, 2002. **244**(2): p. 305-18.
92. Wickham, H., *ggplot2*. 2016.

Figure titles and legends

Figure 1. GRK2 eKO mice display progressive age-related hair loss with early changes in hair follicle morphology and cysts development related to hair cycling. (A) Comparative analysis of dorsal skin appearance at different ages, with detailed 18-mont-old view (right, square area amplified). (B) Representative skin sections showing cumulative alterations in hair follicle homeostasis including cysts at 2-month-old (square area amplified below) before macroscopic alterations are noted. Quantification of cysts/mm of skin observed in GRK2 eKO mice at different ages. As noted in the graph, all GRK2 eKO animals exhibited abnormal cyst-like structures at this stage. (C) Analysis of cyst presence at different ages showed that cysts are absent in newborn or 1st telogen mouse but show a penetrance of 100% after 2nd postnatal anagen. Quantification of cysts/mm of skin observed on GRK2 eKO skin revealed a significant increase in their numbers at p30 (2nd anagen) compared to previous stages (Newborn and 1st telogen). (D)

Schematic view of the differential cycling properties of skin domains. The analysis of their growing pattern in GRK2 eKO animals revealed cyst numbers peak at 8-month-old mice and a preferential growth in cycling anatomical domains such as dorsal compared to resting ear skin. Means ± SEM data are represented, and statistical analysis was performed by 1-way ANOVA followed by Bonferroni's post-hoc test, ****p< 0.0001.

Figure 2. Young GRK2 eKO mice show conserved HFSC pool but deficient anagen induction. (A) Schematic representation of telogen HF structures. Second telogen GRK2 eKO mice show no changes in FACS-sorted $CD34^+$ α6-integrin$^+$ bulge cell numbers. (B) Immunofluorescence analysis confirmed unchanged numbers of bulge Keratin 15^+, $Sox9^+$ or $CD34^+$ cells, in contrast to hair germs (HG), identified by P-cadherin, which are significantly smaller in GRK2 eKO mice. (C) Schematic representation of the depilation-induced hair growth experiment. Second telogen mice (p55) were shaved to induce synchronized growth of back skin HFs. Skin sections were analyzed at p55 and 3 or 8 days after hair removal. (D, E) Proliferation determined by BrdU incorporation is diminished in the HG of GRK2 eKO at early (D+3) (D) or later steps of anagen induction (D+8) (E) compared to control littermates. (F,G) Hair follicle length and presence of pigmented hair shafts were also significantly reduced in GRK2 eKO animals at D+8 stages. Representative images are shown. Means ± SEM data are represented, and statistical analysis was performed using unpaired t-test, **$p < 0.01$, **** $p < 0.0001$.

Figure 3. GRK2 downregulation leads to alterations in signaling pathways involved in stem cell maintenance. (A) Activation status of canonical Wnt/βCat readouts (βCatenin and Lef1) measured by immunofluorescence in p55 mice at different days post-depilation. A deficient activation of this pathway in GRK2 eKO anagen HFs at both D+3 or D+8 is noted compared to control mice. Representative images are shown. (B) Heatmap of differentially expressed genes between GRK2 eKO and Control skin from RNA-seq experiments. Differential expression was assessed from 5 skin samples in each group and upon DESeq2 analysis. (C) Graphical representation of GSEA analysis of RNAseq data from GRK2 eKO versus Control skin. Significant enrichments were observed in either Control (blue) or GRK2 eKO (red) for genesets related to hair follicle function, GPCR, or developmental signaling pathways. The significance is expressed as -log10(FDR).

Figure 4. GRK2 eKO cysts arise from HFSC but are uncoupled from normal hair follicle differentiation and cycling features. (A) Representative schematic of concentric cell layers and their molecular markers thar are normally found in an anagen phase hair follicle (HF). (B) Immunofluorescence analysis of GRK2 KO skin sections reveals that cysts have an epidermal origin (Keratin 5 positive) and appear linked to the stem cell niche (CD34 positive). These structures form a continuous Keratin 6 positive layer with the inner bulge cell niche but do not express the classic HFSC markers CD34 or Keratin 15. Cyst appear as Gata3/CDP negative, indicating the lack of IRS cell fate. (C) Immunodetection of IRS and IRS/Matrix markers Gata3 and CDP reveal a lack of full anagen HF differentiation process in HF-derived cysts (right) compared to normal HF in the same GRK2 eKO animal shown in the left part of the image. (D) During synchronized hair cycle stages, unlike control littermates, GRK2 eKO cysts are proliferative ($Ki67^+$) in catagen and bypass hair cycle regression remaining negative for apoptosis markers (caspase 3) during regression phase. During telogen, cysts are also $Ki67^+$, which indicates that proliferation within these structures is not arrested during the resting phase. Representative immunofluorescence images are shown.

Figure 5. Cysts display lineage infidelity, co-expressing a mixture of IFE, HF and SCC-related tumoral markers. (A) Left, schematic representation of epidermal lineage markers. Right, immunofluorescence analysis shows the presence of cysts cells co-expressing Klf5 and Sox9 transcription factors (detailed in the inset), otherwise distinctly expressed in IFE and HF control cells, suggesting a lineage infidelity phenotype in these cells. The remaining Sox9 expression displayed by cysts cells further supports their follicular origin. (B) Mixed IFE and HF phenotype in cysts is further suggested by the presence of ΔNp63, an IFE marker. (D) Lineage infidelity features in GRK2 eKO cysts are shown together with the expression of tumor-associated markers, as the transcription factor c-Jun or extracellular matrix components such as TnC or αSMA, typical of pro-tumoral environments.

1179 **Figure 6. Dermal Papilla displacement and HFSC structural abnormalities couple cyst emergence**
1180 **with hair loss.** (A) Normal HF morphology with the DP separated from the epidermal compartment by the
1181 α6-integrin$^+$ basement membrane. (B) Histological analysis of 8-month-old GRK2 eKO mouse skin with the
1182 indicated markers showed that cyst growth from the lowest part of the HF displaces the DP (identified as
1183 Lef1$^+$) away from the stem cell niche. Representative immunofluorescence images are shown. (C)
1184 Histochemical analysis of 8-month-old skin sections with the indicated markers showed miss-organization
1185 of both bulge cell layers which are no longer visible and appear interspersed in cyst-linked GRK2 eKO HFs.
1186 Marked structural alterations in bulge structure at 8-month-old GRK2 e KO mice were detected with
1187 immunofluorescence staining of key cell-cell junction proteins and cytoskeletal components. (D) These
1188 alterations led to loss of CD34 HFSC canonical marker in 18-month-old mutant mice compared to controls,
1189 together with the disappearance of the classical bulge morphology. (E) Quantification of bulge numbers
1190 revealed a decline in their amount specifically in GRK2 eKO animals during aging, a phenomenon not
1191 observed in control littermates. Representative immunofluorescence images are shown. Means ± SEM data
1192 are represented, and statistical analysis was performed by 1-way ANOVA followed by Bonferroni's post-
1193 hoc test, **$p < 0.01$, ***$p < 0.001$, ****$p < 0.0001$.
1194
1195 **Figure 7. Epidermal cysts are destroyed during aging in a mechanism resembling immune-mediated**
1196 **alopecia.** (A) Right graph shows that total number of cysts peak at 8M of age and then decrease by 18M.
1197 Left image indicates that cysts but not bulges attract immune infiltrate. In contrast to controls, where the
1198 presence of immune cells is restricted to the infundibular region, cysts are largely infiltrated by CD45$^+$
1199 immune cells. (B) According to their morphology and structural integrity, cysts were classified in "healthy"
1200 ones (blue) with round morphology and surrounding CD45$^+$ cells, "compromised" cysts (yellow) that have
1201 started losing their morphology and are infiltrated by immune cells, and "destroyed" ones (red) formed by
1202 remnants free in the dermis. The number of the two later types increases with age, consistent with the
1203 evolution of the number of these structures with age shown in panel above. (C) Destroyed cysts (red arrow
1204 in lower right panel) are observed as structures lacking intercellular E-cadherin junctions, in contrast to the
1205 healthy-looking ones (blue arrow) that are positive for this marker. Quantification of cysts/mm of skin
1206 observed in GRK2 eKO mice at different ages. (D) Apoptotic cell markers such as cleaved caspase 3 or
1207 TUNEL were detected together with γ-H2AX within destroyed cysts, indicating that they are destroyed
1208 during aging. (E) Immune cells infiltrating cysts assessed with the indicated specific markers. CD3$^+$ T cells
1209 are located in the surrounding dermis, consistent with the observed high expression of T-cell adhesion
1210 molecules (ICAM1). Antigen Presenting Cells (MHC-II$^+$) and F4/80$^+$ macrophages were also detected in
1211 infiltrated cysts. ((F) A gene expression signature of overexpressed genes in GRK2 eKO (GRK2 eKO
1212 signature) was enriched in alopecia samples obtained in the C3H mouse model (left panel), and in skin punch
1213 biopsy samples from AA patients (right panel). (G) A gene expression signature of overexpressed genes in
1214 human AA patients (human AA signature) was enriched in GRK2 eKO skin. Box and whiskers plots are
1215 used with means and min to max data are represented, and statistical analysis was performed by 1-way
1216 ANOVA followed by Bonferroni's post-hoc test, ** $p < 0.01$, *** $p < 0.001$.
1217
1218